EFFECT OF SELF-STRATIFICATION OF SEDIMENT SUSPENSIONS IN TURBULENT PLANE COUETTE FLOW

BY

RUIYU WANG

DISSERTATION

Submitted in partial fulfillment of the requirements
for the degree of Doctor of Philosophy in Environmental Engineering in Civil Engineering
in the Graduate College of the
University of Illinois at Urbana-Champaign, 2013

Urbana, Illinois

Doctoral Committee:

Professor Gary Parker, Chair, Director of Research
Professor Marcelo H. Garcia
Professor Kenneth T. Christensen
Professor Arthur R. Schmidt

ABSTRACT

The research of this dissertation is motivated by the problem of the formation and breakup of lutoclines in tidal flows. Sediment delivered by rivers into sea spread on the continental shelves, and are resuspended by waves or tidal currents. The sediment concentration near the bottom can be enhanced to a fairly high level, and a sharp concentration gradient known as a lutocline forms between a bottom layer and an upper layer, which dampens turbulence and inhibits mixing. As a result, most sediment will be confined in the lower layer, which is referred to as a fluid mud layer. The turbulence structure, velocity profile and suspended sediment concentration profile is remarkably different depending whether or not a lutocline is present. In tidal environments, a lutocline can be formed as sediment settles out during stagnant high or low tide, and then broken up by strong flow velocities generated by rising or ebbing tide.

A preliminary to the study of lutocline formation and breakup by studying the stable stratification in steady, equilibrium sediment-laden plane turbulent Couette flow is presented in the dissertation. Analysis has been made based on a mixing length hypothesis, and numerical simulations have been conducted with an algebraic turbulence closure model and a stratification-corrected k-ε Reynolds Averaged Navier-Stokes Model (RANS).

The results show that in sediment-laden turbulent plane Couette flow where density stratification effect can be neglected, the relation between the mean velocity and the roughness height takes a form similar to the Keulegan relation for open channel flow, differing only by a constant. The eddy viscosity profile can be fitted to a quadric polynomial, similar to the parabolic profile in open channel flow. Based on this, the equilibrium sediment concentration profile for cases of negligible stratification effect can be derived in a similar way to the Rousean profile for open channel flow.

In the case of sediment-laden flow, two dimensionless parameters have been identified to govern the self-stratification of the sediment-laden turbulent plane Couette flow: a shear Richardson number $\mathbf{Ri}_\tau$ and a dimensionless fall velocity $\widehat{v_s}$. Increase in either parameter has a similar effect of strengthening sediment stratification, which is manifested by a sharpening of concentration gradient near the bottom, and a preferential dampening of turbulence in the lower layer of the flow. The relation between the friction and the layer-averaged flow velocity is determined with regression, showing increase in either $\mathbf{Ri}_\tau$ or $\widehat{v_s}$ result in reduction of resistance. Similarly, the relation between the layer averaged concentration and the

parameters $\mathbf{Ri}_\tau$ and $\widehat{v_s}$ is determined with regression and reduces to the relation for non-stratified flow as the stratification effect diminishes.

Although the setting of the numerical model constrains that the sediment can not settle out of the computation domain, in cases of sufficiently high sediment stratification or insufficient shear stress, sediment is sequestered in a thin layer near the bed, which in fact represents a condition that not all sediment can be held in suspension. A maximum value of the product of $\mathbf{Ri}_\tau$ and $\widehat{v_s}$ is given as a criterion above which sediment could not be held in suspension.

ACKNOWLEDGMENTS

During my study in University of Illinois at Urbana-Champaign, I have received a lot of help. I owe many thanks to my research advisors, Professor Gary Parker and Professor Marcelo H. Garcia. I appreciate very much my committee members, Professor Arthur Schmidt and Professor Kenneth Christensen for their guidance and support. I also greatly appreciate the help I received during my research from my fellow graduate students and post-docs including Esther Eke, Tzu-hao Yeh, Matthew Czapiga, Enrica Viparelli, Andrew Rehn, Anna Pelosi, Zhenduo Zhu, Octavio Sequeiros, Eduardo Puhl, Blake Landry, Xiaofeng Liu, Dingbao Wang, J. Ezequiel Martin, Davide Motta, Som Dutta, Tatiana Garcia McKay, Namjeong Choi, Andrea Zimmer, Viviana Morales, Hiroshi Miwa, Jose Mier, Summit Sinha, Talia Tokyay. I also very much appreciate the help I received from Ven Te Chow Laboratory Researcher Andrew Waratuke and Lab secretary Robin Ray. Thanks to ExxonMobil Corporation for providing me with the financial support to complete this project. And finally, thanks to my family and friends who offered so much support and love to me.

TABLE OF CONTENTS

CHAPTER 1

INTRODUCTION

When delivered by rivers into coastal water, sediment-laden buoyant flumes spread offshore and alongshore on the surface of the sea, then gradually deposit on the sea bottom, usually within the continental shelf. This is because sediment-laden river water usually has a lower density than the salty sea water (Wright and Nittrouer, 1995). River water with very high sediment concentration can immediately plunge to the bottom of sea as a hyperpycnal flow. In either case, within the continental shelf the deposited sediment can be resuspended by waves or tidal currents. In some cases, the sediment concentration near the bottom can be enhanced to a fairly high level by resuspension, sometimes to 10 - 100 g/l, which is 4-5 orders of magnitude greater than the concentration on the surface (Ross and Mehta, 1989).

If a sharp concentration gradient between a bottom layer and an upper layer forms, it can dampen turbulence and inhibit mixing. As a result, most sediment will be confined in the lower layer. The lower layer is then referred to as a fluid mud layer, and the interface between the fluid mud layer and the upper layer is called a lutocline. The turbulence structure, velocity profile and suspended sediment concentration profile is remarkably different depending whether or not a lutocline is present. As a result, an understanding of the mechanism of lutocline and fluid mud formation is important in the study of sediment transport and morphodynamics in the estuarine and coastal environment. The fluid mud layer has a significant damping effect on the energy of incoming waves (Sheremet and Stone, 2003). Fluid mud layers are especially common in estuaries with abundent fine sediment input (Winterwerp, 1999; Zhang, et al., 2001). On the Amazon shelf, fluid mud thickness can be on the order of several meters near the salinity front (Kineke, et al., 1996).

A lutocline is a zone of sharp density gradient mediated by variation in the concentration of suspended sediment. It falls in the general category of pycnoclines in general, such as temperature-mediated thermoclines and salt-mediated haloclines. The case of sediment, however, is particularly interesting because the flow makes its own stratification; the flow suspends the sediment, which then damps the turbulence of the flow. The present work was motivated by the problem of the formation and breakup of lutoclines in tidal flows. A lutocline can be formed as sediment settles out during stagnant high or low tide, and then is broken up by strong flow velocities generated by rising or ebbing tide (Hsu, T., et al., 2007).

Plane turbulent Couette flow provides a natural setting for studying the formation and breakup of lutoclines. The flow and suspension can be driven by the oscillation of a top plate. The oscillation can be terminated, allowing the sediment to settle out and form a lutocline. The oscillation can then be recommenced, causing the eventual breakup of the lutocline.

Turbulent Couette flows have been investigated by a number of researchers. Bech et al. (1995) investigated the turbulent Couette flow at low Reynolds number with experiments and DNS simulations. Frohn et al. (2010) computed the velocity profile of gas plane Couette flow. Lei et al. (2011) computed the velocity profile in a mesoscale plane Couette flow using the technique of dissipative particle dynamics. Ko et al. (2011), Becker and McKinley, (2000) and Vergori (2010) also studied the characteristics of plane Couette flow, including the velocity and concentration profiles, but only in cases of laminar flow. Garcia-Villalba et al. (2011) used Direct Numerical Simulation to study density-stratified turbulent Couette flow and demonstrated how the scale of the turbulence structures are suppressed by the stratification.

The present analysis represents a preliminary to the study of lutocline formation and breakup. Here the case of steady, equilibrium sediment-laden plane turbulent Couette flow is considered. Three flow models are employed: a mixing length model, an algebraic turbulence closure of Gelfenbaum and Smith (1986) for stratified flow, and a stratification-corrected k-ε Reynolds Averaged Navier-Stokes Model (RANS) (Rodi, 1993). The contribution of this study is instead of focusing on the detail turbulence structures of the flow, the sediment-laden turbulent plane Couette flow is studied as a whole. A quasi-Rousean sediment concentration profile is derived based on general behavior of the turbulent plane Couette flow. The study also captures salient parameters governing flow self-stratification and turbulence damping. Relations between these parameters and the depth-averaged velocity and concentration are generalized. A criterion determining whether turbulence can be sustained and sediment can be held in suspension is also given based on these parameters.

CHAPTER 2

DESCRIPTION OF THE MODELS

The turbulence structure, velocity profiles and suspended sediment concentration distributions in turbulent plane Couette flow at equilibrium is obtained by implementing a numerical model over time until it reaches a steady state. Figure 1 shows the Couette flow and computational domain. The surfaces of the upper and lower plates have the same roughness height k_s. The lower plate is not moving, and a given shear stress is applied to the upper plate so as to move it at speed U_T. In the figure, τ is shear stress, u is flow velocity, z is the vertical coordinate, ρ is water density, ν is the kinematic viscosity of the water, ν_t is a turbulent eddy viscosity and $u_* = \sqrt{\tau / \rho}$ is the shear velocity. In general, the shear stress is given as (1):

$$\tau = \rho\left(\nu + \nu_t\right)\frac{\partial u}{\partial z} = \rho u_*^2 \tag{1}$$

At equilibrium conditions, the shear stress throughout the water column is a constant value equal to the value applied at the upper plate.

Here the problem is solved using two turbulence closure models: the algebraic closure model of Gelfenbaum-Smith (Gelfenbaum and Smith, 1986) and the k-ε model (Rodi, 1993; see also Jones and Launder, 1972). The governing equations of the k-ε model are:

$$\frac{\partial u}{\partial t} = \frac{\partial}{\partial z}\left(\nu + \nu_t\right)\frac{\partial u}{\partial z} \tag{2}$$

$$\frac{\partial c}{\partial t} + v_s\frac{\partial c}{\partial z} = \frac{\partial}{\partial z}\left(\frac{\nu_t}{\sigma}\frac{\partial c}{\partial z}\right) \tag{3}$$

$$\frac{\partial k}{\partial t} = \frac{\partial}{\partial z}\left(\frac{\nu_t}{\sigma_k} + \nu\right)\frac{\partial k}{\partial z} + \nu_t\left(\frac{\partial u}{\partial z}\right)^2 + \frac{Rg\nu_t}{\sigma}\frac{\partial c}{\partial z} - \varepsilon \tag{4}$$

$$\frac{\partial \varepsilon}{\partial t} = \frac{\partial}{\partial z}\left(\frac{\nu_t}{\sigma_\varepsilon} + \nu\right)\frac{\partial \varepsilon}{\partial z} + C_{1\varepsilon}\frac{\varepsilon}{k}\left(\nu_t\left(\frac{\partial u}{\partial z}\right)^2 + \frac{C_{3\varepsilon}Rg\nu_t}{\sigma}\frac{\partial c}{\partial z}\right) - C_{2\varepsilon}\frac{\varepsilon^2}{k} \tag{5}$$

where t is time, k is the turbulent kinetic energy per unit volume, ε is a corresponding dissipation rate per unit volume of turbulent kinetic energy, σ, σ_ε and σ_k are appropriate Schmidt numbers, g is the acceleration of gravity, R is the submerged specific gravity of sediment (e.g. 1.65 for quartz), c is the volume suspended sediment concentration, v_s is the settling velocity of the sediment and $C_{1\varepsilon}$ etc. are

standard closure coefficients (Rodi, 1993). The closure is completed by assuming the following form for the eddy viscosity:

$$\nu_t = C_\mu \frac{k^2}{\varepsilon} \tag{6}$$

In the k-ε model, the parameters σ, σ_k, σ, C_μ, $C_{1\varepsilon}$, $C_{2\varepsilon}$, $C_{3\varepsilon}$ are given as:

$\sigma = 0.85$, σ_k=1, σ_ε=1.3, C_μ=0.09, $C_{1\varepsilon}$=1.44, $C_{2\varepsilon}$=1.92, $C_{3\varepsilon}$=0

The domain of computation is the water column excluding two wall regions close to the top and bottom plates, because the standard k-ε model is valid only for fully turbulent flow (Beausoleil-Morrison, et al., 1998). The thickness of each of these layers, which are not included in the present model, is denoted as b.

The variables are made dimensionless as follows:

$$\hat{z} = \frac{z}{h},\ \hat{u} = \frac{u}{u_{*n}},\ \widehat{u_*} = \frac{u_*}{u_{*n}},\ \hat{t} = \frac{u_{*n}}{h}t,\ \widehat{k_s} = \frac{k_s}{h},\ \hat{b} = \frac{b}{h},\ \widehat{\nu_t} = \frac{\nu_t}{hu_{*n}},\ \hat{c} = \frac{c}{C},\ \widehat{\nu_s} = \frac{\nu_s}{u_{*n}},\ \hat{k} = \frac{k}{u_{*n}^2},$$

$$\hat{\varepsilon} = \frac{h\varepsilon}{u_{*n}^3}, \widehat{U_T} = \frac{U_T}{u_{*n}} \tag{7}$$

Here h is the gap height between the two plates and C is the layer-averaged volume concentration of suspended sediment, which is specified as a given parameter:

$$C = \frac{\int_b^{h-b} c dz}{h - 2b} \tag{8}$$

u_{*n} is the shear velocity at the upper plate under equilibrium conditions when equilibrium is reached. U_T stands for the top plate velocity, while the lower plate is taken to be fixed. Two possible implementations are possible here. That is, at the top plate, either u_{*n} or U_T may be specified and the other calculated. Here all calculations are performed using a specified value of u_{*n}, corresponding to a specified applied shear stress at the upper plate. Therefore, u_{*n} is equivalent to u_* in the following context.

The dimensionless forms of the governing equations become:

$$\frac{\partial \hat{u}}{\partial \hat{t}} = \frac{\partial}{\partial \hat{z}}\left(\widehat{\nu_t} + \frac{1}{\mathbf{Re}_\tau}\right)\frac{\partial \hat{u}}{\partial \hat{z}} \tag{9}$$

$$\frac{\partial \hat{c}}{\partial \hat{t}} + \widehat{\nu_s}\frac{\partial \hat{c}}{\partial \hat{z}} = \frac{\partial}{\partial \hat{z}}\left(\frac{\widehat{\nu_t}}{\sigma}\frac{\partial \hat{c}}{\partial \hat{z}}\right) \tag{10}$$

$$\frac{\partial \hat{k}}{\partial \hat{t}} = \frac{\partial}{\partial z}\left(\frac{\widehat{\nu_t}}{\sigma_k} + \frac{1}{\mathbf{Re}_\tau}\right)\frac{\partial \hat{k}}{\partial \hat{z}} + \widehat{\nu_t}\left(\frac{\partial \hat{u}}{\partial \hat{z}}\right)^2 + \mathbf{Ri}_\tau \frac{\widehat{\nu_t}}{\sigma}\frac{\partial \hat{c}}{\partial \hat{z}} - \hat{\varepsilon} \tag{11}$$

$$\frac{\partial \hat{\varepsilon}}{\partial \hat{t}} = \frac{\partial}{\partial \hat{z}}\left(\frac{\widehat{\nu_t}}{\sigma_\varepsilon} + \frac{1}{\mathbf{Re}_\tau}\right)\frac{\partial \hat{\varepsilon}}{\partial \hat{z}} + C_{1\varepsilon}\frac{\hat{\varepsilon}}{\hat{k}}\left(\widehat{\nu_t}\left(\frac{\partial \hat{u}}{\partial \hat{z}}\right)^2 + \mathbf{Ri}_\tau \frac{C_{3\varepsilon}\widehat{\nu_t}}{\sigma}\frac{\partial \hat{c}}{\partial \hat{z}}\right) - C_{2\varepsilon}\frac{\hat{\varepsilon}^2}{\hat{k}} \tag{12}$$

In the above relations, the shear Reynolds number $\mathbf{Re}_\tau = \frac{u_* h}{\nu}$, the shear Richardson number $\mathbf{Ri}_\tau = \frac{RCgh}{u_*^2}$, and the dimensionless eddy viscosity is given by:

$$\widehat{\nu_t} = C_\mu \frac{\hat{k}^2}{\hat{\varepsilon}} \tag{13}$$

The flow within the two near-wall regions is assumed to obey the logarithmic law for hydraulically rough, turbulent flow. The boundary conditions are thus given as:

$$\widehat{u_b} = \widehat{u_*}\left(\frac{1}{\kappa}\ln\left(\frac{\hat{b}}{\widehat{k_s}}\right) + B_s\right) \quad \text{at } \hat{z} = \hat{b} \tag{14}$$

$$\widehat{u_t} = \widehat{U_T} - \widehat{u_*}\left(\frac{1}{\kappa}\ln\left(\frac{\hat{z}}{\widehat{k_s}}\right) + B_s\right) \quad \text{at } \hat{z} = 1 - \hat{b} \tag{15}$$

$$\frac{\partial \hat{u}}{\partial \hat{z}} = \frac{\widehat{u_*}}{\kappa \hat{b}}, \text{ at } \hat{z} = \hat{b}, \qquad \frac{\partial \hat{u}}{\partial \hat{z}} = -\frac{\widehat{u_*}}{\kappa \hat{b}}, \text{ at } \hat{z} = 1 - \hat{b} \tag{16}$$

$$\hat{k} = \frac{\widehat{u_*}^2}{\sqrt{C_\mu}}, \text{ at } \hat{z} = \hat{b}, \qquad \hat{k} = \frac{\widehat{u_*}^2}{\sqrt{C_\mu}}, \text{ at } \hat{z} = 1 - \hat{b} \tag{17}$$

$$\hat{\varepsilon} = \frac{\widehat{u_*}^3}{\kappa \hat{b}}, \text{ at } \hat{z} = \hat{b} \qquad \hat{\varepsilon} = \frac{\widehat{u_*}^3}{\kappa \hat{b}}, \text{ at } \hat{z} = 1 - \hat{b} \tag{18}$$

The boundary conditions for $\hat{k}$ and $\hat{\varepsilon}$ are deduced from turbulent boundary layer theory. At the boundaries of the turbulent plane Couette flow, the characteristic mean strain rate S can usually be characterized by $\frac{\partial u}{\partial z}$, which is much greater than any other component in the strain rate tensor. According to the assumption of k-ε model,

$$\langle u'v' \rangle = u_*^2 = C_\mu \frac{k^2}{\varepsilon} S \tag{19}$$

Here, u' stands for the fluctuating velocity in the x direction, and v' stands for the fluctuating velocity in the z directiong. $\langle u'v' \rangle$ is the dominant component of the Reynolds stress in the x direction. The brackets denote averages over turbulence. The production rate of turbulence P is given by:

$$P = \langle u'v' \rangle S \tag{20}$$

It is assumed that in the boundary region at equilibrium $P \approx \varepsilon$. Therefore, substituting (20) into (19) gives:

$$|\langle u'v' \rangle| = C_\mu \frac{k^2}{|\langle u'v' \rangle| S} S \tag{21}$$

This results in the relation

$$k = \frac{u_*^2}{\sqrt{C_\mu}} \tag{22}$$

Supposing the logarithmic velocity profile to prevail in the boundary regions, the strain rate at distance b from the wall is $S \approx \frac{\partial u}{\partial z} = \frac{u_*}{\kappa b}$; substituting (22) into (19), the boundary condition on ε is given as:

$$\varepsilon = \frac{u_*^3}{\kappa b} \tag{23}$$

Upon nondimensionalization, (22) and (23) reduce to the forms (17) and (18).

Here, $\widehat{u_b}$ and $\widehat{u_t}$ stand for the dimensionless velocity $\hat{u}$ at the bottom and the top of the computation domain, i.e. $\hat{u}$ at $\hat{z} = \hat{b}$ and $\hat{z} = 1 - \hat{b}$ respectively. Their values are determined by $\widehat{u_*}$ and $\widehat{U_T}$, but only one of these two can be used as a boundary condition. Nevertheless when the equilibrium state is reached, the following relations must hold:

$$\widehat{u_t} - \widehat{u_b} = \int_{\hat{b}}^{1-\hat{b}} \frac{\widehat{u_*}^2}{\widehat{\nu_t} + \frac{1}{\mathbf{Re_\tau}}} dz \tag{24}$$

$$\widehat{u_t} + \widehat{u_b} = \widehat{U_T} \tag{25}$$

Between (25) - (24), (14) and (15), the following relation is obtained:

$$2\widehat{u_*}\left(\frac{1}{\kappa} \ln\left(\frac{\hat{b}}{\widehat{k_s}} \right) + 8.5 \right) = \widehat{U_T} - \widehat{u_*}^2 \int_{\hat{b}}^{1-\hat{b}} \frac{1}{\widehat{\nu_t} + \frac{1}{\mathbf{Re_\tau}}} dz \tag{26}$$

This provides a relation between $\widehat{u_*}$ and $\widehat{U_T}$. Thus if one of these is specified at the top as a boundary condition, the other can be computed at any time from (26). As noted above, all calculations here are performed under the condition of specified, constant applied shear stress at the upper plate, in which case $\widehat{u_*}$ is defined and $\widehat{U_T}$ is computed from (26).

The Gelfenbaum-Smith (Gelfenbaum and Smith, 1986) model is a zero-equation turbulence model which takes the stratification into account through an algebraic closure. In the model the eddy viscosity profile $\widehat{\nu_{t0}}$ for the clear water case is computed, and then the gradient Richardson number is given as

$$\mathbf{Ri}_g = -\mathbf{Ri}_\tau \frac{\dfrac{d\hat{c}}{d\hat{z}}}{\left(\dfrac{d\hat{u}}{d\hat{z}}\right)^2} \tag{27}$$

The eddy viscosity is computed as:

$$\widehat{\nu_t} = \frac{\widehat{\nu_{to}}}{1+10X} \quad , \quad X = \frac{1.35\,\mathbf{Ri_g}}{1+1.35\,\mathbf{Ri_g}} \tag{28}$$

The problem can be solved iteratively from a clear-water first guess of the eddy viscosity.

In the present analysis, the total mass of suspended sediment in the water column is preserved, so that sediment is neither eroded from or deposited onto the bed. Referring to (8), this results in the constraint

$$\frac{1}{1-2\hat{b}}\int_{\hat{b}}^{1-\hat{b}} \hat{c}\,d\hat{z} = 1 \tag{29}$$

CHAPTER 3

RESULTS

3.1 Results for sediment-free plane turbulent Couette flow

Turbulent Couette flow with zero concentration is first simulated with the k-ε model. The boundary conditions were evaluated using either of the value $\hat{b} = b/k = 0.01$ or 0.05, as indicated below. The reason for using different values of $\hat{b}$ is that a wide range of $\widehat{k_s}$ has been applied in the simulations, and for a good reason $\hat{b}$ should be greater than $\widehat{k_s}$. Results of the profiles for $\hat{u}$, $\hat{k}$, $\hat{\varepsilon}$, and $\widehat{\nu_t}$, are shown in Figure 2. It can be seen in the figure that the results of turbulent Couette flow are antisymmetric about the centerline in velocity; and symmetric about the centerline in kinetic energy, dissipation rate and eddy viscosity. This is due to the symmetric nature of the boundary conditions.

From the point of view of dimensional analysis, the physical variables of interest in this problem are: u_*, h, z, k_s, ν, ν_t, ρ, D_s and C, where D_s denotes particle size (so that a particle with size D_s and submerged specific gravity R has fall velocity v_s). The independent physical units are L, T, M. Therefore, six dimensionless groups can be formed. We use the following six dimensionless parameters defined in (7) to characterize the behavior of the problem: $\hat{z}$, $\widehat{\nu_t}$, $\mathbf{Re}_\tau$, $\widehat{k_s}$, $\mathbf{Ri}_\tau$, $\widehat{v_s}$.

Here $\widehat{v_s}$ and $\mathbf{Ri}_\tau$ are related to the size and layer-averaged concentration of the sediment, respectively, while the other dimensionless numbers are related to the characteristics of the flow. Of particular interest is the dimensionless eddy viscosity $\widehat{\nu_t} = \dfrac{\nu_t}{hu_*}$. The eddy diffusivity of suspended sediment ν_{tc} is often assumed to be proportional to the eddy viscosity, and thus equals ν_t/σ, where σ is the sediment Schmidt number. Once the eddy viscosity profile is known, then the equilibrium concentration profile in turbulent Couette flow can be expressed in a form corresponding to the case of the Rousean distribution in open channel flow (Rouse, 1937):

$$\hat{c} = \widehat{c_b} \exp\left(-\widehat{v_s}\sigma \int_{\frac{1}{2}}^{\hat{z}} \frac{1}{\widehat{\nu_t}} d\hat{z} \right) \tag{30}$$

From dimensional analysis, the following relation should exist:

$$\widehat{\nu_t} = f\left(\hat{z}, \widehat{k_s}, \mathrm{Re}_\tau, \mathbf{Ri}_\tau, Z\right) \tag{31}$$

In the case of zero concentration, $\widehat{\nu_s}$ and $\mathbf{Ri}_\tau$, which are related to the characteristics of sediment, can be omitted, so that:

$$\widehat{\nu_t} = f\left(\hat{z}, \widehat{k_s}, \mathbf{Re_\tau}\right) \tag{32}$$

Similar to the case of open channel flow, the profile of eddy viscosity can also be analyzed in terms of the shear stress and velocity profiles. Prandtl's mixing length hypothesis (Prandtl, 1925) is adopted here to express the velocity profile:

$$\tau = \rho l^2 \left(\frac{\partial u}{\partial z}\right)^2 \tag{33}$$

$$l=\kappa z,\ u_*^2 = \frac{\tau}{\rho} \tag{34}$$

$$u_* = \kappa z \frac{\partial u}{\partial z} \tag{35}$$

Here l refers to the Prandtl's mixing length. This hypothesis leads to the logarithmic velocity profile under the condition of constant shear stress over the boundary layer. This condition is not valid in the case of open channel flow, to which it is often applied. In the case of steady plane Couette flow, however, the shear stress is indeed constant. So it is reasonable to assume the following logarithmic velocity profile as a zeroth-order approximation:

$$\frac{u}{u_*} = \frac{1}{\kappa}\ln\left(\frac{z}{k_s}\right) + B_s \qquad (0<z<h/2) \tag{36}$$

$$\frac{u}{u_*} = \frac{2}{\kappa}\ln\left(\frac{h}{2k_s}\right) - \frac{1}{\kappa}\ln\left(\frac{(h-z)}{k_s}\right) + B_s \qquad (h/2<z<h) \tag{37}$$

The profile given by (36) and (37) is continuous and smooth in the entire domain. Assuming $\nu_t + \nu \approx \nu_t$, the following eddy viscosity profile is derived:

$$\widehat{\nu_t} = \kappa \hat{z} \qquad (0<z<h/2) \tag{38}$$

$$\widehat{\nu_t} = \kappa\left(1-\hat{z}\right) \qquad (h/2<z<h) \tag{39}$$

The profile of eddy viscosity given by (38) and (39) is only a crude approximation of the one predicted by, e.g. the k-ε model. However, it suggests that $\widehat{\nu_t}$ is a function only of $\hat{z}$, and is not related to $\widehat{k_s}$ and $\mathbf{Re}_\tau$.

To test this hypothesis, various combinations of $\widehat{k_s}$ and $\mathbf{Re}_\tau$ have been applied in simulations of sediment-free plane, turbulent Couette flow. In these calculations, $\widehat{k_s}$ ranges from 0.0002 to 0.01, and $\mathbf{Re}_\tau$ ranges from 500 to 20000.

In Figure 3 velocity profiles are expressed as $\hat{u} - \widehat{U}$ (horizontal axis) versus $\hat{z}$ (vertical axis), where $\widehat{U}$ stands for the depth-averaged velocity, defined as

$$\hat{U} - \frac{1}{1-2\hat{b}} \int_{\hat{b}}^{1-\hat{b}} \hat{u} d\hat{z} \tag{40}$$

Two lines are shown in Figure 3. One corresponds to the logarithmic approximation of (36) and (37), and the other corresponds to all the simulation results for 10 pairs of values of ($\widehat{k_s}$, $\mathbf{Re}_\tau$). The velocity profiles for all of these pairs plot on top of each other, indicating that the velocity profile is not dependent on the values of these two parameters over the tested range.

Due to the invariance of the dimensionless velocity profile to variation in both $\widehat{k_s}$ and $\mathbf{Re}_\tau$ over the range studied, a friction law can be derived for which $\widehat{U} = U/u_*$ is a function of $\widehat{k_s}$ only. As shown in Figure 4, the relation obtained by k-ε simulations can be fitted accurately with a logarithmic relation:

$$\frac{U}{u_*} = \frac{1}{\kappa} \ln\left(\frac{19.6h}{k_s}\right) \tag{41}$$

The relation is very similar to the Keulegan (1938) relation of open-channel flow, for which h refers to the flow depth, and 19.6 becomes 11.

Figure 5 shows plots of velocity profiles for a) turbulent open channel flow and b) plane turbulent Couette flow. The simulations were performed with the values ($\widehat{k_s}$, $\mathbf{Re}_\tau$) = (0.01, 35000) for open channel flow and ($\widehat{k_s}$, $\mathbf{Re}_\tau$) = (0.01, 1000) for plane Couette flow, where in defining these two parameters, h refers to gap height in the case of plane Couette flow and depth in the case of open channel flow. For the case of open channel flow, the logarithmic law is compared with the results of the k-ε formulation, as obtained using the software of Yeh and Parker (2011). Figure 5 shows that the results of open channel flow and turbulent Couette flow are similar and both largely follow the logarithmic law. In the case of open channel flow the k-ε model predicts a wake region where the velocity deviates from the logarithmic law. No such wake region is evident for the case of plane Couette flow.

Figure 6 shows the "theoretical" eddy viscosity profile given by (38) and (39), which results from an imposition of the logarithmic law to plane Couette flow, the standard parabolic eddy viscosity profile of open channel flow (Rouse, 1937) and computational results obtained from the k-ε model using the following combinations of $\widehat{k_s}$ and $\mathbf{Re}_\tau$: (0.0002,1000), (0.0005,1000), (0.001,1000), (0.002,1000), (0.005,1000), (0.01,1000), (0.002, 500), (0.002,2500), (0.002,10000), (0.002,20000). All the results for the k-ε model fall nearly on top of each other, with only the result of $\mathbf{Re_\tau}$ =500 showing some deviation.

It can be therefore be concluded that $\widehat{\nu_t}$ can be regarded as independent of $\widehat{k_s}$ and $\mathbf{Re_\tau}$ when $\mathbf{Re_\tau} \geq 1000$, a range within which the flow is fully turbulent. The "theoretical" profile, the open channel eddy viscosity profiles and the computed profiles have almost the same gradient at the upper and lower boundaries. While the eddy viscosity profile of open channel flow is commonly approximated as parabolic, satisfying the relation

$$\widehat{\nu_t} = \kappa \hat{z}\left(1-\hat{z}\right) \tag{42}$$

(Rouse, 1937), the eddy viscosity profile of the Couette flow obtained from the present calculations is best represented by the following fourth-order polynomial:

$$\widehat{\nu_t} = \widehat{\nu_{t0}}\left(1-5\left(\hat{z}-0.5\right)^2+4\left(\hat{z}-0.5\right)^4\right) \tag{43}$$

Here, $\widehat{\nu_{t0}}$ = 0.13697 is the maximum value of $\widehat{\nu_t}$ at $\hat{z}=0.5$. Numerical tests show that the form of **(43)** is not dependent on the selection of $\hat{b}$.

3.2 Quasi-Rousean Concentration Profile

The classical equilibrium concentration profile for suspended sediment in open channel flow is the Rousean profile (Rouse, 1937). It is based on the assumption of a) vanishing self-stratification effects due to suspended sediment, and b) a parabolic eddy viscosity satisfying (42), where again *h* is interpreted as flow depth rather than gap height in interpreting the dimensionless parameters.

A corresponding form can now be derived for plane Couette flow. At steady state, (3) reduces to

$$\widehat{v_s}\hat{c}+\frac{\widehat{\nu_t}}{\sigma}\frac{\partial \hat{c}}{\partial \hat{z}}=0 \tag{44}$$

Integration of (44) gives

$$\hat{c} = \widehat{c_{\frac{1}{2}}} \exp\left(-\widehat{\nu_s}\sigma \int_{\frac{1}{2}}^{\hat{z}} \frac{1}{\widehat{\nu_t}} d\hat{z} \right) \tag{45}$$

where $\widehat{c_{\frac{1}{2}}}$ denotes the value of $\hat{c}$ at $\hat{z} = \frac{1}{2}$. The above formulation is valid whether or not sediment stratification effects prevail. Because of the symmetric nature of the computational domain, the relative concentration at the middle of the water column $\widehat{c_{\frac{1}{2}}}$ is used as a reference concentration. The neglect of stratification effects allows representation of the eddy viscosity profile with (43). Substituting (43) into (45), the following concentration profile can be derived analytically:

$$\hat{c} = \widehat{c_{1/2}} \left(\frac{\left(3 - 2\hat{z}\right)\hat{z}^2}{\left(1 + 2\hat{z}\right)\left(1 - \hat{z}\right)^2} \right)^{-\frac{\sigma \widehat{\nu_s}}{6\widehat{\nu_{tc}}}} \tag{46}$$

From the normalization condition (29), the reference concentration at $\hat{z} = 0.5$ is given by:

$$\widehat{c_{1/2}} = \frac{1}{\int_{\hat{b}}^{1-\hat{b}} \left(\frac{\left(3 - 2\hat{z}\right)\hat{z}^2}{\left(1 + 2\hat{z}\right)\left(1 - \hat{z}\right)^2} \right)^{-\frac{\sigma \widehat{\nu_s}}{6\widehat{\nu_{tc}}}} d\hat{z}} \tag{47}$$

The concentration profile given by (46) can be called the quasi-Rousean plane Couette sediment concentration profile, because of its similarity to the form of the classical Rousean sediment concentration profile of open channel flow. The quasi-Rousean concentration profiles in the lower half of the turbulent Couette flow are compared with the Rousean concentration profiles in open channel flow in Figure 7 - Figure 9. Here, h_* refers to the water depth for the case of open channel flow, and half of the gap height h for the case of plane turbulent Couette flow. It can be seen here that for all values of $\widehat{v_s} = v_s/u_*$, the open channel Rousean profile and the plane Couette quasi-Rousean profile give similar results close to the bottom. They begin to show noticeable deviation above $\hat{z} = 0.15$. At values of $\widehat{v_s}$ as high as $\widehat{v_s} = 1$, the two profiles are very close to each other throughout the entire depth. The curves representing them fall almost completely on each other in Figure 9.

3.3 Results for fully-stratified flow

In this section, several cases of fully-stratified sediment-laden plane Couette flow are analyzed with the k-ε model. The effect of stratification is taken into account by the terms including $\frac{\partial \hat{c}}{\partial \hat{z}}$ in equations (11) and (12). It can be therefore inferred that it is the dimensionless numbers $\mathbf{Ri}_\tau$ and $\widehat{v_s}$ that determine the level of stratification. Indeed, these parameters enter into the formulation as the product $\mathbf{Ri}_\tau \widehat{v_s}$ in (11) and (12).

Figure 10 shows the results for $\mathbf{Ri}_\tau$ = 291.36, v_s/u_* = 0.026, and $\widehat{k_s} = 0.0005$ when a steady state is reached. Figure 10(a) shows the velocity profile, 10(b) the concentration profile, 10(c) the turbulent kinetic energy profile, 10(d) the dissipation rate of kinetic energy profile, 10(e) the eddy viscosity profile and 10(f) the shear velocity profile. Here, the shear stress is represented in terms of the local shear velocity u_*, which facilitates comparison with the shear velocity at the boundary u_{*n}. By comparing Figure 10 with Figure 2, it can be seen that the symmetry of the profiles of turbulent kinetic energy, dissipation rate of turbulent kinetic energy and eddy velocity are broken in the case of fully stratified flow.

Figure 10(b) shows that the concentration profile in fully-stratified flow clearly deviates from the quasi-Rousean profile. The results of the k-ε model and the algebraic Gelfenbaum-Smith model, however, agree quite well. Figure 10(e) shows that the eddy viscosity in fully-stratified flow is significantly damped compared with non-stratified flow. The damping effect is stronger in the lower half of the flow where the concentration gradient is greater than in the upper half. Figure 10(f) shows that the shear stress in the entire water column is indeed equal to the shear stress at the boundary, which is a necessary condition for equilibrium flow.

The dimensionless number $\mathbf{Ri}_\tau$ reflects the ratio between the buoyancy force, which resists vertical mixing, and the shear force which provides energy to hold sediment in suspension. The effect of varying $\mathbf{Ri}_\tau$ is shown in Figure 11 - Figure 14, where $\widehat{v_s}$ is kept equal 0.018, $\widehat{k_s}$ equal 0.01 and $\hat{b}$ equal 0.01. Figure 11 shows the eddy viscosity profiles, Figure 12 shows the velocity profiles ands Figure 13 shows the concentration profiles, all for several values of $\mathbf{Ri}_\tau$. Figure 14 shows a comparison between the concentration profiles predicted by the k-ε model, the Gelfenbaum-Smith model and the quasi-Rousean solution for $\mathbf{Ri}_\tau$=437.

Figure 11 shows that the eddy viscosity profile computed by the fully-stratified model converges to the profile of sediment-free plane Couette flow at low values of $\mathbf{Ri_\tau}$. As $\mathbf{Ri_\tau}$ increases, the eddy viscosity profile computed for fully stratified sediment-laden plane Couette flow deviates from the non-stratified profile. For low values of $\mathbf{Ri_\tau}$, it is symmetrical around $\hat{z} = 0.5$, similar to the non-stratified profile. As $\mathbf{Ri_\tau}$ increases, the eddy viscosity is gradually damped, with a bias toward the lower half. Equations (9) and (10) show that the damping effect of concentration stratification is related to the concentration gradient itself..

Figure 12 shows flow velocity profiles in the fully-stratified plane Couette flow. Damping of turbulence results in flow velocities that are greater than in the case of non-stratified plane Couette flow. This is because the eddy viscosity is reduced as $\mathbf{Ri_\tau}$ increases. Similar to the eddy viscosity profiles, the velocity profile converges to the result of non-stratified plane Couette flow at low values of $\mathbf{Ri_\tau}$.

Figure 13 shows the concentration profiles for various $\mathbf{Ri_\tau}$ computed with the fully stratified model in comparison with the quasi-Rousean concentration profile. The results for the fully-stratified model again converge to the quasi-Rousean concentration profile as $\mathbf{Ri_\tau}$ becomes small. Indeed, the concentration profile does not deviate much from the quasi-Rousean profile for $\mathbf{Ri_\tau} < 100$. At high values of $\mathbf{Ri_\tau}$, the results of the fully-stratified model deviate substantially from the quasi-Rousean profile, and show a concentration gradient in the lower half of the flow that is greater than in the upper half. It can be seen by comparing Figures 11 with Figure 13 that a) the concentration gradient in the lower half is greater than the upper half at high $\mathbf{Ri_\tau}$ values, corresponding to b) greater damping of turbulence in the lower half of the concentration profile than in the upper half.

Figure 14 shows that for a high value of $\mathbf{Ri_\tau} = 437$, the results of the k-ε model agree well with the results of the Gelfenbaum-Smith model, while both deviate very substantially from the quasi-Rousean profile. More specifically, stratification concentrates the suspended sediment near the bed by damping vertical mixing.

The effect of varying $\widehat{v_s}$, i.e. the ratio of fall velocity to shear velocity**,** is shown in Figure 15 - Figure 18, with the other parameters set at $\widehat{k_s}$ equal 0.01, $\hat{b}$ equal 0.01 and $\mathbf{Ri_\tau}$ equal 48.56. Figures 15, 16 and 17 show, respectively, the effect of varying $\widehat{v_s}$ while holding $\mathbf{Ri_\tau}$ constant on eddy viscosity, velocity and suspended sediment concentration profiles. A comparison of Figure 15 with Figure 11, Figure 16 with Figure 12 and Figure 17 with Figure 13 shows a general symmetry: increasing $\widehat{v_s}$ under the constraint of

constant $\mathbf{Ri_\tau}$ shows essentially the same damping effect as increasing $\mathbf{Ri_\tau}$ under the constraint of constant $\widehat{v_s}$. At large values of $\widehat{v_s}$, the eddy viscosity and velocity profiles show more asymmetry than at large values of $\mathbf{Ri_\tau}$. The increase of flow velocity at high values of $\widehat{v_s}$, however, is not as much as at high values of $\mathbf{Ri_\tau}$.

Figure 17 shows the concentration profiles for various values of $\widehat{v_s}$. It is seen here that if the fall velocity is low compared to the shear velocity, the concentration profile is almost uniform throughout the entire water depth. This uniformity however soon breaks down as fall velocity increases. When the fall velocity increases to about 10% of the shear velocity, the concentration near the bottom reaches as much as 20 times the concentration near the top, and the concentration gradient in the lower half is significantly higher than in the upper half. This corresponds to the asymmetry of the eddy viscosity and velocity profile seen at high values of $\widehat{v_s}$.

Figure 18 compares the concentration profiles provided by k-ε model, Gelfenbaum-Smith model, and quasi-Rousean profile for various values of $\widehat{v_s}$ at a constant value of $\mathbf{Ri_\tau}$ equal 48.56. It can be seen here that for low values of $\widehat{v_s}$, the results of the k-ε model agree relatively well with the quasi-Rousean solution, whereas for high values of $\widehat{v_s}$, the result of the k-ε model agrees relatively well with the Gelfenbaum-Smith model.

In a previous section, it has been shown that the results for non-stratified turbulent plane Couette flow are not dependent on $\widehat{k_s}$ (Figure 3). It is therefore natural to raise the question as to whether the results of fully-stratified plane Couette flow also show this lack of dependence on $\widehat{k_s}$. Figure 19 shows the results for fully-stratified plane Couette flow with $\mathbf{Ri_\tau}$ = 291.36, $\widehat{v_s}$ = 0.026, $\widehat{k_s}$ ranging from 0.0005 to 0.05 and $\hat{b}$ is set equal 0.05 in all simulations. It can be seen here that the velocity profiles for various values of $\widehat{k_s}$ have identical shapes, only translating in magnitude. This translation reflects the higher wall resistance associated with higher values of $\widehat{k_s}$, in correspondence to the dependence on $\widehat{k_s}$ in (41) for the case of unstratified flow. All the other profiles, i.e. the concentration, turbulent kinetic energy, dissipation rate of turbulent kinetic energy, eddy viscosity and shear velocity profiles, are essentially identical for all values of $\widehat{k_s}$.

As can be seen from Figures 12, 13, 16 and 17, the dimensionless mean velocity and concentration in the turbulent plane Couette flow vary substantially with variation in the dimensionless parameters $\mathbf{Ri_\tau}$ and $\widehat{v_s}$. These trends can be captured in terms of generalized regression relations. Figure 20 and Figure 21 show the general pattern of dependence of the dimensionless mean velocity of the plane Couette flow on dimensionless parameters $\mathbf{Ri_\tau}$ and $\widehat{v_s}$. It can be seen in Figure 20 and Figure 21 that the relations for both $\widehat{U}$ versus $\widehat{v_s}$ and $\widehat{U}$ versus $\mathbf{Ri_\tau}$ converge to a single point when both $\widehat{v_s}$ and $\mathbf{Ri_\tau}$ approach zero (clear water conditions). The relation between the dimensionless mean velocity and roughness height in clear water is given by (41). Based on the fact that $\mathbf{Ri_\tau}$ and $\widehat{v_s}$ occur as a product in (11) and (12), a relation of the following form can be found for turbulent plane Couette flow.

$$\widehat{U} = f\left(\widehat{k_s}\right) + a\mathbf{Ri}_{\boldsymbol{\tau}}\widehat{v_s} \tag{48}$$

Here the first term on the right-hand side of (48) denotes the clear-water dependence, the second term captures stratification effects, and a is a parameter to be determined. Figure 22 shows that the dependence of $\widehat{U}$ on the product of $\widehat{v_s}$ and $\mathbf{Ri_\tau}$ is largely valid, and is captured with a value of a determined from linear regression to be 1.4735. Therefore the regression relation for the dimensionless mean velocity versus the dimensionless parameters $\mathbf{Ri_\tau}$ and $\widehat{v_s}$ is

$$\widehat{U} = \frac{1}{\kappa}\ln\left(\frac{19.6}{\widehat{k_s}}\right) + 1.4735 Ri_\tau \widehat{v_s} \tag{49}$$

with the coefficient of determination $R^2 = 0.9781$

A predictive relation for the layer-averaged concentration C can be obtained by means of normalization with the near-bed concentration, i.e. C/c_b. The near-bed concentration is here represented by the concentration at a reference height b. All the calculations presented in this section were performed with $\hat{b} = 0.01$. If the concentration is low enough so that the effect of stratification can be neglected, C/c_b will be given by the quasi-Rousean solution (46), which can alternatively be expressed as:

$$\frac{C}{c_b} = f\left(\widehat{v_s}\right) = \frac{\displaystyle\int_{\hat{b}}^{1-\hat{b}} \left(\frac{\left(3-2\hat{z}\right)\hat{z}^2}{\left(1+2\hat{z}\right)\left(1-\hat{z}\right)^2}\right)^{-\frac{\sigma}{6\widehat{\nu_{tc}}}\widehat{v_s}} d\hat{z}}{\left(\dfrac{\left(3-2\hat{b}\right)\hat{b}^2}{\left(1+2\hat{b}\right)\left(1-\hat{b}\right)^2}\right)^{-\frac{\sigma}{6\widehat{\nu_{tc}}}\widehat{v_s}}} \tag{50}$$

It is thus reasonable to assume that the relation between C / c_b and the dimensionless numbers of $\widehat{v_s}$ and $\mathbf{Ri}_\tau$ that includes the effects of stratification would take the form

$$\frac{C}{c_b} = f\left(\widehat{v_s}\right) + g\left(\widehat{v_s}, \mathbf{Ri}_\tau\right) \tag{51}$$

The form of the regression relation corresponding to (51) is found to be

$$\frac{C}{c_b} = f\left(\widehat{v_s}\right) + \left(1.893\left(\frac{v_s}{u_*}\right)^2 - 0.435\left(\frac{v_s}{u_*}\right) - 0.0114\right)\widehat{v_s}\mathbf{Ri}_\tau \tag{52}$$

Figure 23 and Figure 24 show the relation between C / c_b and the dimensionless parameters $\mathbf{Ri}_\tau$ and $\widehat{v_s}$. It can be seen here that the curves representing the regression and simulation almost all fall together except a bit discrepancy at high $\mathbf{Ri}_\tau$ and low $\widehat{v_s}$, showing that the regression fits the data acquired from numerical simulation pretty well. When $\mathbf{Ri}_\tau$=0, (52) reduces to (50), the analytically derived concentration profile for negligible stratification. The relation of (50) is represented by the points at $\mathbf{Ri}_\tau = 0$ in Figure 24.

Since $\mathbf{Ri}_\tau$ and $\widehat{v_s}$ occur as a product in (11) and (12), Figure 25 shows the values of C / c_b acquired from simulation and regression (52) versus $\widehat{v_s}\,\mathbf{Ri}_\tau$. It can be seen that the data points representing simulation results and regression results are clearly paired, and most of the pairs are very close together. Those pairs of data points that are not very close together are connected with a bar. The coefficient of determination of the regression (52) is $R^2 = 0.9928$.

It was found in this study that a solution for equilibrium stratification is not always attainable. In cases of sufficiently high stratification, the turbulence is not capable of holding the sediment in suspension, and instead the sediment is sequestered in a thin layer near the bed. Although sediment cannot deposit on the bed in the present model because of the constraint (29), this sequestration effectively corresponds to a condition at which the sediment cannot be held in suspension. It is therefore interesting to investigate the criterion beyond which this sequestration occurs. All the data points in Figure 23, 24 and 25 represent cases for which sediment could be held in suspension.

Figure 26 represents the projection of the simulation results onto the $\mathbf{Ri}_\tau$ - $\widehat{v_s}$ plane. Here crosses represent cases for which sediment could not be held in suspension, and dots represent cases for which it

was held in suspension. It is seen in Figure 26 that the boundary between these two regimes can be roughly given by the following relation:

$$Ri_\tau \widehat{v_s} = 7 \tag{53}$$

That is (53) gives the criterion above which sediment cannot be held in suspension in turbulent plane Couette flow. From this relation it is easy to derive a relation for the maximum attainable suspended sediment concentration in turbulent plane Couette flow:

$$C_{\max} = \frac{7u_*^3}{Rghv_s} \tag{54}$$

Figure 27 shows the maximum concentration that can be reached in a turbulent plane Couette flow for various grain sizes, assuming R = 2.65. Here, C = 0.25 is deemed as the maximum concentration that is physically possible. Zhang (1961) has derived a suspended sediment transport capacity equation in open channel flow using an energy method:

$$C_{\max} = K\left(\frac{U^3}{ghv_s}\right)^m \tag{55}$$

In the above relation, K and m are empirical parameters, with $0.4 < m < 1.5$, and U is the mean flow velocity of open channel flow. It is interesting to note the similarity between (54) and (55), even though a) they apply to different flows (plane Couette flow versus open channel flow) and b) different approaches have been employed to derive them.

It should be pointed out that (54) defines a concentration limit defined by stratification effects. It should be noted, however, that turbulence is damped at sufficiently high concentrations, even in the absence of stratification effects. This mode of damping is not considered in the present analysis.

CHAPTER 4

CONCLUSIONS

Plane, turbulent Couette flow represents a simple configuration for the study of sediment suspensions. This is because at steady-state conditions, the shear stress is constrained to be constant in the vertical. Here equilibrium, sediment-laden turbulent Couette flows have been analyzed using a) a mixing length closure, b) the Gelfenbaum-Smith algebraic turbulence closure (Gelfenbaum and Smith, 1986), which includes density stratification effects, and c) the stratification-corrected k-ε model RANS model of turbulent flow (Rodi, 1993).

The following key results were obtained.

1. For the case of sediment-free flow, the friction relation (41) can be defined which differs from the Keulegan (1938) relation for open channel flow only by a constant.
2. In the case of sediment-free flow, the profile of eddy viscosity can be fitted to the quartic polynomial (43), a form that is similar to the parabolic profile of open channel flow.
3. The Rousean profile for suspended sediment concentration of open channel flow is derived under the assumption that density stratification effects can be neglected. A corresponding quasi-Rousean profile for suspended sediment concentration in turbulent plane Couette flow, (46), can be obtained from considerations of mass balance of suspended sediment and relation (43) for eddy viscosity.
4. Density stratification effects due to sediment suspension are mediated by two parameters, a shear Richardson number $\mathbf{Ri}_\tau$ and a dimensionless fall velocity $\widehat{v_s}$. An increase in $\mathbf{Ri}_\tau$ at constant $\widehat{v_s}$, corresponding to e.g. increasing layer-averaged suspended sediment concentration, has an effect on the flow that is similar to an increase in $\widehat{v_s}$ at constant $\mathbf{Ri}_\tau$. This is because the two parameters appear as a product in (11) and (12).
5. The effects of increasing stratification are manifested in terms of a) a preferential damping of turbulence in the lower layer of the flow, and b) a corresponding sharpening of the suspended sediment concentration profile there.
6. The analysis leads to the determination of the relation (49) for friction and the relation (52) for layer-averaged suspended sediment concentration, both of which reduce to the appropriate forms for negligible stratification effects, but which capture the stratification effects embodied in increasing $\mathbf{Ri}_\tau$ and $\widehat{v_s}$.

7. Finally, the analysis provides a criterion beyond which stratification effects are so strong that all the sediment is sequestered in a very thin layer near the bed. This condition effectively corresponds to the inability of the flow to hold maintain an equilibrium suspension at sufficiently high values of $\mathbf{Ri}_\tau$ and $\widehat{\nu_s}$.

Acknowledgement

This research was funded by ExxonMobil Corporation.

Notations

a	a parameter relating the depth averaged velocity to $\mathbf{Ri}_\tau$ and $\widehat{\nu_t}$
b	reference height
$\hat{b}$	dimensionless reference height
B_s	constant in logarithmic velocity profile
C	mean concentration in the computation domain
$\hat{c}$	normalized local concentration
$\widehat{c_{\frac{1}{2}}}$	normalized local concentration at the middle of the computation domain
$C_{1\varepsilon}, C_{2\varepsilon}, C_{3\varepsilon}, C_\mu$	standard closure coefficients of k-ε model
c_b	local concentration at reference height
C_{max}	maximum mean concentration in turbulent plane Couette flow
D_s	sediment particle size
ε	dissipation rate of turbulent kinetic energy per unit volume
$\hat{\varepsilon}$	dimensionless dissipation rate of turbulent kinetic energy per unit volume
h	distance between the upper and lower plate
k	turbulent kinetic energy per unit volume
K	an empirical parameter of Zhang (1961)
$\hat{k}$	dimensionless turbulent kinetic energy per unit volume
k_s	roughness height
$\widehat{k_s}$	dimensionless roughness height
κ	von Karman concstant
l	Prandtl's mixing length

m	an empirical parameter of Zhang (1961)
ν	kinematic viscosity of water
ν_t	turbulent eddy viscosity
$\widehat{\nu_t}$	dimensionless turbulent viscosity
$\widehat{\nu_{t0}}$	maximum value of $\widehat{\nu_s}$ in non-stratified turbulent plane Couette flow
ν_{tc}	eddy diffusivity of suspended sediment
P	production rate of turbulence per unit volume
R	submerged specific gravity of sediment
R^2	coefficient of determination of regression
$\mathbf{Re}_\tau$	shear Reynolds number
$\mathbf{Ri}_\mathrm{g}$	gradient Richardson number
$\mathbf{Ri}_\tau$	shear Richardson number
ρ	water density
S	mean strain rate
σ	sediment Schmidt number
σ_ε	ε Schmidt number
σ_k	k Schmidt number
t	time
$\hat{t}$	dimensionless time
τ	shear stress
u	flow velocity
$\hat{u}$	dimensionless flow velocity
$\widehat{U}$	Depth averaged velocity
$\widehat{u_b}$	dimensionless velocity at the lower boundary of computation domain
$\widehat{u_t}$	dimensionless velocity at the upper boundary of computation domain
U_T	upper plate speed
$\widehat{U_T}$	dimensionless upper plate speed
$\langle u'v' \rangle$	Reynolds stress in the x direction
u_*	shear velocity
$\widehat{u_*}$	dimensionless shear velocity
u_{*n}	equilibrium shear velocity at the upper plate

v_s	settling velocity of sediment
$\widehat{v_s}$	dimensionless settling velocity
z	vertical coordinate
$\hat{z}$	dimensionless vertical coordinate

REFERENCES

Beausoleil-Morrison, I. and Clarke, J. 1998. The implications of using the standard k–ε turbulence model to simulate room air flows which are not fully turbulent. Proceedings of ROOMVENT '98, Stockholm: 99–106.

Bech, K. H., Tillmark, N., Alfredsson, P. H. and Andersson, H. I. 1995. An investigation of turbulent plane Couette flow at low Reynolds numbers. Journal of Fluid Mechanics, 286, 291-325.

Becker, L. E. and McKinley, G. H. 2000. The stability of viscoelastic creeping plane shear flows with viscous heating. Journal of Non-Newtonian Fluid Mechanics, 92(2), 109-133.

Frohn, A., Roth, N., Anders, K. 2010. Heat Atlas: M10 Heat Transfer and Momentum Flux in Rarefied Gases. Springer Verlag, Stuttgart.

Hsu, T.J., Traykovski, P.A., Kineke, G.C. 2007. On modeling boundary layer and gravity-driven fluid mud transport. Journal of Geophysical Research, 112, C04011.

Garcıa-Villalba, M., Azagra, E. and Uhlmann, M. 2011. A numerical study of turbulent stably-stratified plane couette flow. W.E. Nagel et al. (eds.), High Performance Computing in Science and Engineering '10, ,DOI 10.1007/978-3-642-15748-619, Springer-Verlag Berlin Heidelberg.

Gelfenbaum, G. and Smith, J. D. 1986. Experimental evaluation of a generalized suspended-sediment transport theory. In Shelf and Sandstones, Canadian Society of Petroleum Geologists Memoir II, Knight, R. J. and McLean, J. R., eds., 133 – 144.

Jones, W.P. and Launder, B.E. 1972. The Prediction of laminarization with a two-equation model of turbulence. International Journal of Heat and Mass Transfer, 15: 301-314.

Keulegan, G.H. 1938. Laws of turbulent flow in open channels. Journal of the National Bureau of Standards, Research Paper 1151, 21, 707-741, Washington, D.C.

Kineke, G.C., Sternberg, R.W., Trowbridge, J.H., and Geyer, W.R. 1996. Fluid-mud processes on the Amazon continental shelf. Continental Shelf Research, 16(5/6): 667-696

Ko, J., Lucor, D. and Sagaut, P. 2011. Effects of base flow uncertainty on Couette flow stability. Computers & Fluids, 43(1), 82-89.

Lei, H., Fedosov, D. A. and Karniadakis, G, E. (2011) Time-dependent and outflow boundary conditions for Dissipative Particle Dynamics. Journal of Computational Physics, 230(10): 3765-377

Prandtl, L. 1925. Über die ausgebildete Turbulenz, Z. Angew. Math. Mech., 5, 136, 1925.

Rodi, W. 1993.Turbulence models and their application in hydraulics—A state-of-the-art review, 3rd Ed. A.A.Balkema Publishers,VT.104 p.

Ross, M.A. and Mehta. 1989. On the mechanics of lutoclines and fluid mud. Journal of Coastal Research, Special Issue, 5: 51-61.

Rouse, H. 1937. Modern conceptions of the mechanics of fluid turbulence. Trans. Am. Soc. Civ. Eng.TACEAT0066-0604, 102, 463–554.

Sheremet, A. and Stone, G. 2003. Observations of nearshore wave dissipation over muddy sea beds. Journal of Geophysical Research Oceans. Vol. 108, Issue C11. 21:1-11.

Vergori, L. 2010. Flows at small Reynolds and Froude numbers, International Journal of Engineering Science, 48(11), 1659-1670

You, Zai-Jin, and B. S. Yin. 2007. Direct measurement of bottom shear stress under water waves. Journal of Coastal Research, SI 50: 1132-1136.

Zhang Q., Wu Y., Lian J. and Ding P. 2001. Modeling of the high concentration layer of cohesive sediment under the action of waves and currents, International Journal of Sediment Research, 16(2), 215-223.

Zhang, R. 1961. River Dynamics. Beijing: China Industry Press.

Wright, L.D., and Nittrouer, C.A. 1995. Dispersal of river sediments in coastal seas: six contrasting cases. Estuaries, 18: 494-508.

FIGURES

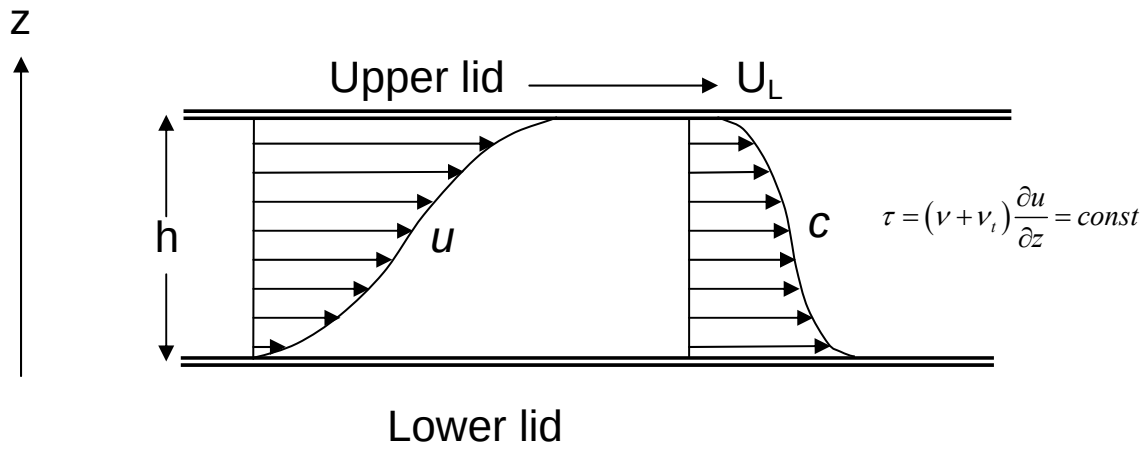

Figure 1. Computational domain for plane turbulent Couette flow

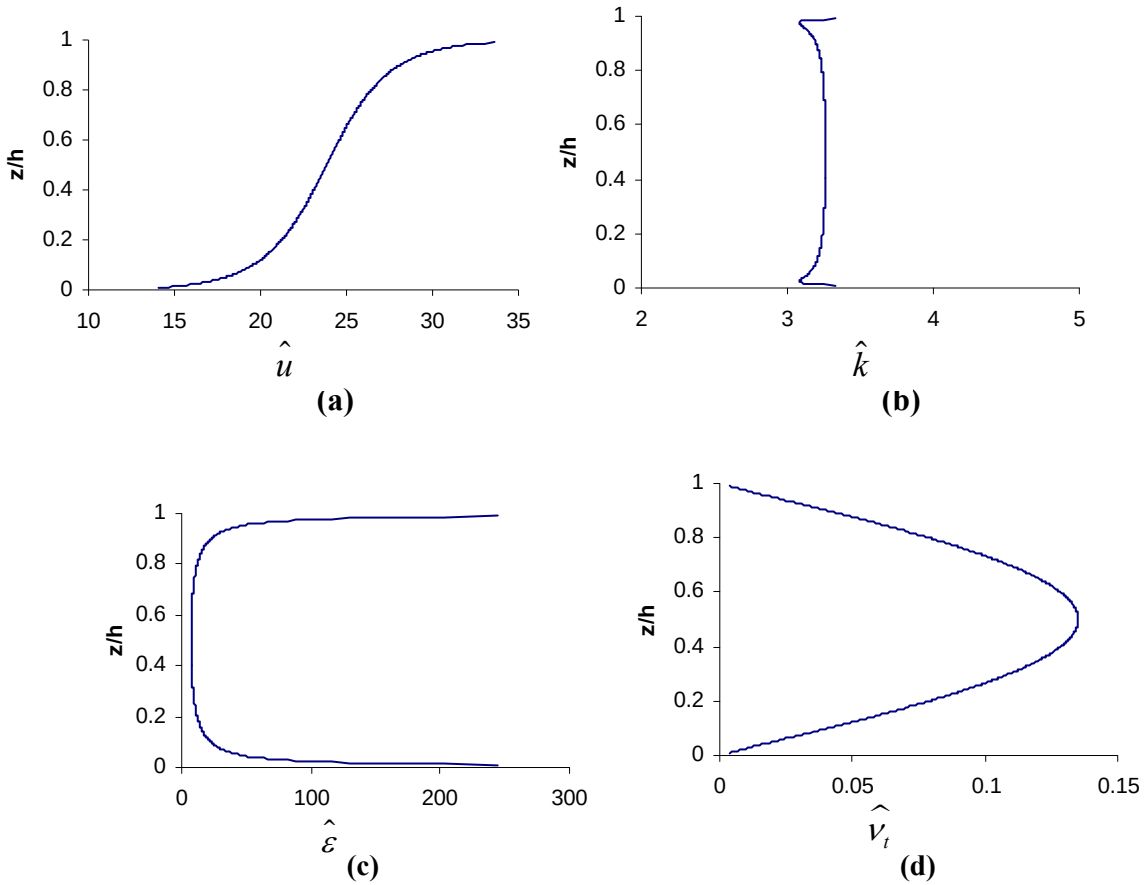

Figure 2. Results of calculations for sediment-free plane turbulent Couette flow with zero suspended sediment concentration, with $\hat{k}_s$ =0.01 and $\hat{b}$ =0.01 (a) velocity; (b) turbulent kinetic energy; (c) dissipation rate of turbulent kinetic energy and (d) turbulent viscosity

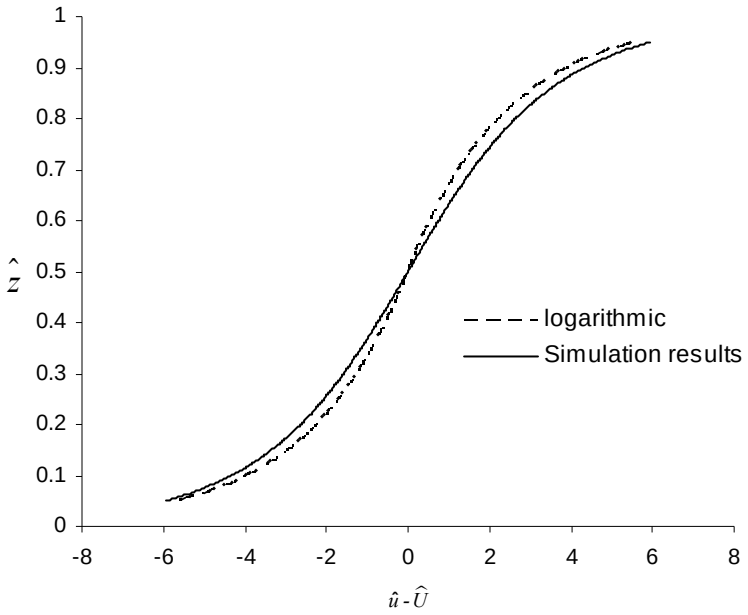

Figure 3. Results of velocity profiles obtained from the k-ε model with 10 combinations of $\widehat{k_s}$ and Re_τ, along with the paired logarithmic profiles of (20) and (21). The profiles for all ten of the combinations of ($\widehat{k_s}$, Re_τ) plot on top of each other, indicating the insensitivity of the velocity profile to these parameters. The combinations of ($\widehat{k_s}$, Re_τ) are: (0.0002, 1000), (0.0005, 1000) , (0.001, 1000) , (0.002, 1000) , (0.005, 1000), (0.01, 1000), (0.002, 2500), (0.002, 10000), (0.002, 20000), (0.002, 500), and $\hat{b}$ =0.01

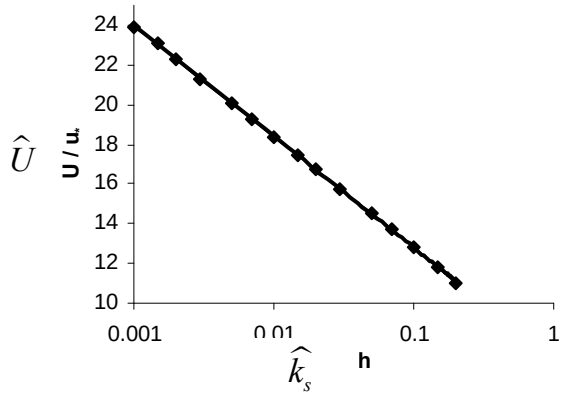

Figure 4. Relation between the dimensionless layer-averaged mean velocity $\widehat{U}$ and the relative roughness height $\widehat{k_s}$ for the case of plane turbulent sediment-free Couette flow

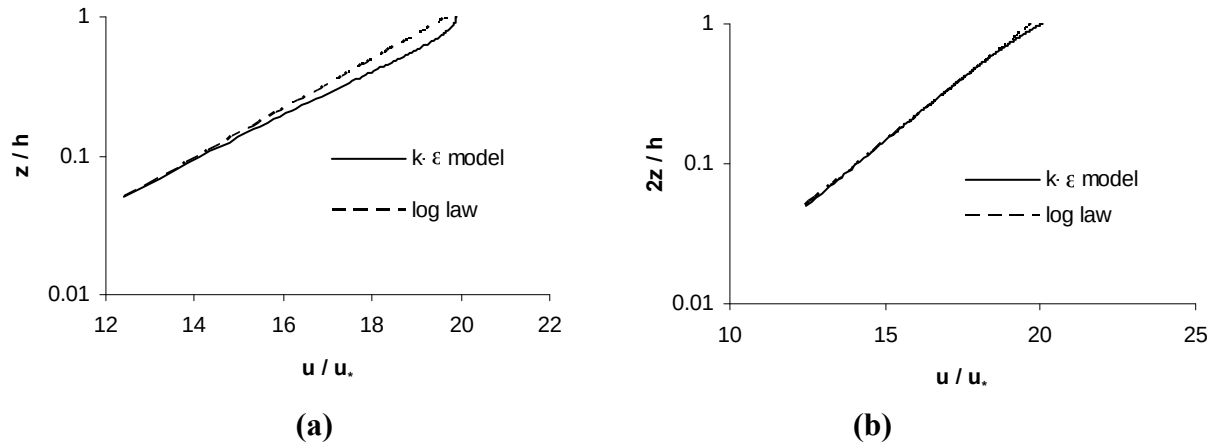

Figure 5. Results of k-ε model, along with the logarithmic law for (a) open channel flow (Yeh, 2011) and (b) the lower half of plane, turbulent Couette flow with $\widehat{k_s}$ =0.01 and $\hat{b}$ =0.05

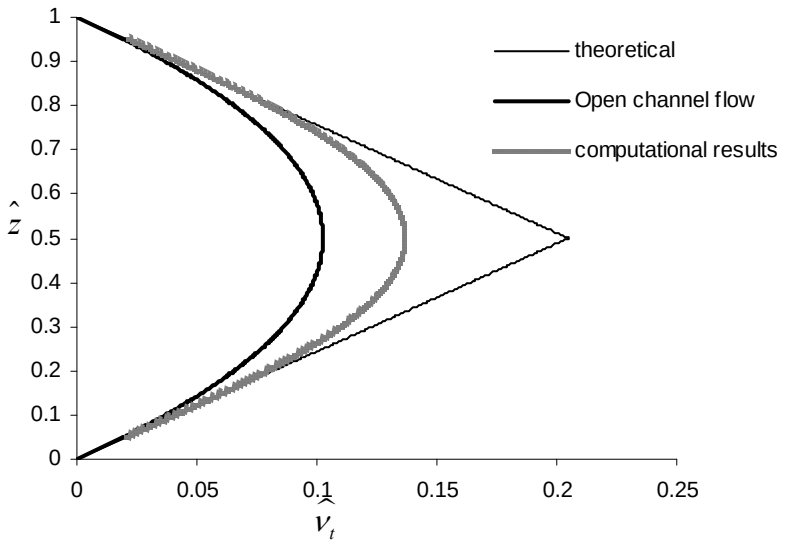

Figure 6. Eddy viscosity profiles for various combinations of $\widehat{k_s}$ and Re_τ ; with the "theoretical" profile given by (4.22) and (4.23), as well as the parabolic profile corresponding to open channel flow under the assumption of a logarithmic velocity profile. The values of ($\widehat{k_s}$ Re_τ) used were (0.0002,1000), (0.0005,1000), (0.001,1000), (0.002,1000), (0.005,1000), (0.01,1000), (0.002, 500), (0.002,2500), (0.002,10000), (0.002,20000) and $\hat{b}$ =0.01 All the results from the k-ε formulation plot nearly on top of each other

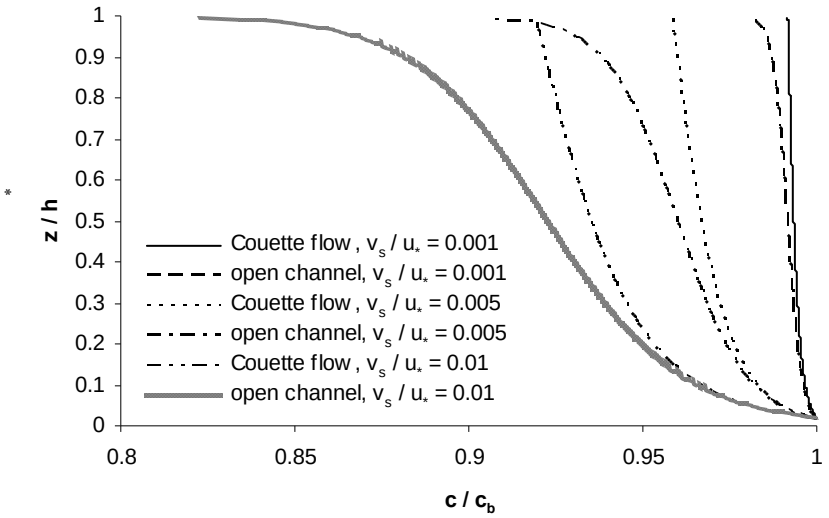

Figure 7. Comparison between the Rousean concentration profile for open channel flow and the quasi-Rousean concentration profile for the lower half of plane turbulent Couette flow, $\widehat{v_s}$ =0.001, 0.005, 0.01

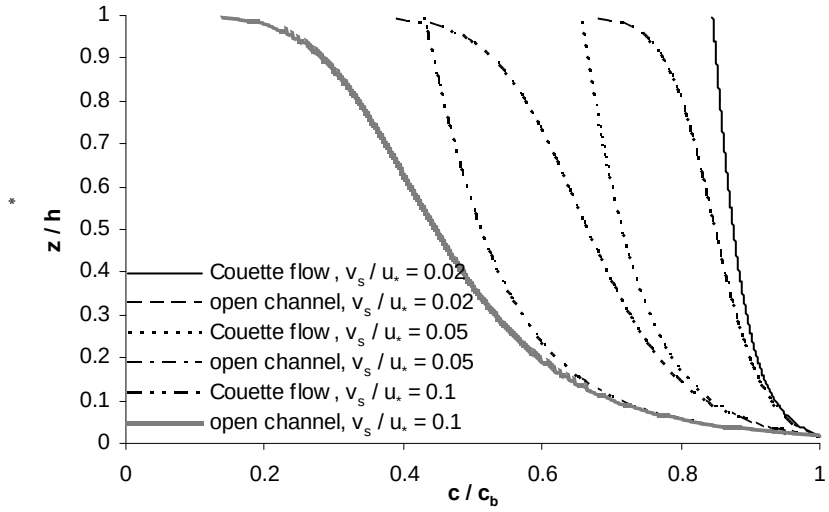

Figure 8. Comparison between the Rousean concentration profile for open channel flow and the quasi-Rousean concentration profile for the lower half of plane turbulent Couette flow, $\widehat{v_s}$ =0.02, 0.05, 0.1

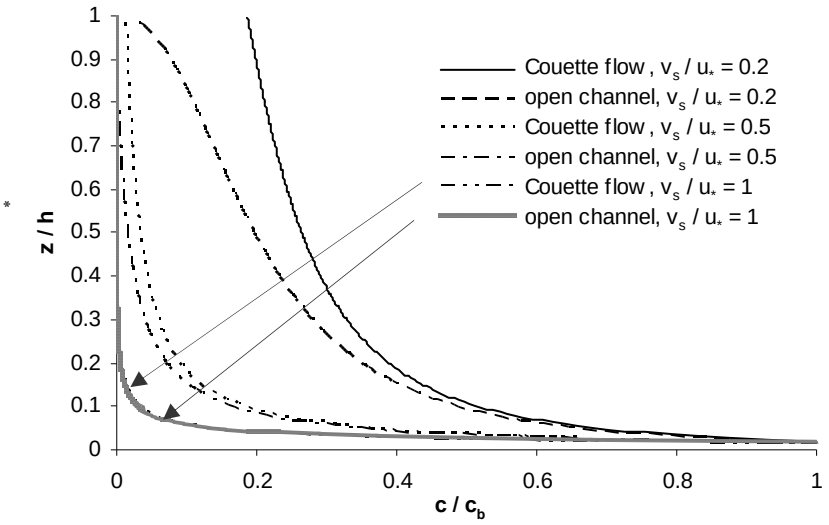

Figure 9. Comparison between the Rousean concentration profile for open channel flow and the quasi-Rousean concentration profile for the lower half of plane turbulent Couette flow, $\widehat{v_s}$ =0.2, 0.5, 1

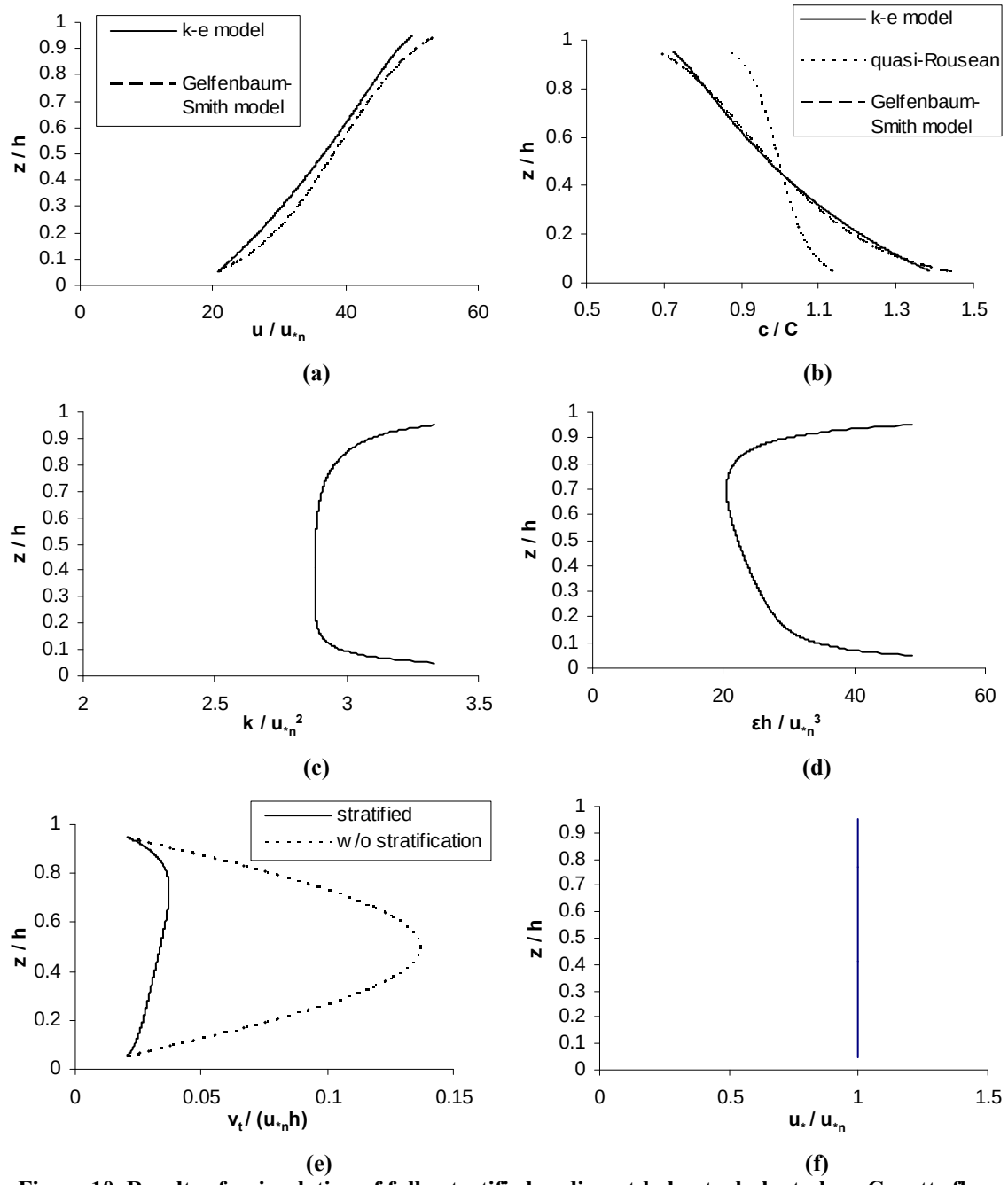

Figure 10. Results of a simulation of fully-stratified, sediment-laden turbulent plane Couette flow, for the parameters Ri_τ = 291.36, $\widehat{\nu_s}$ = 0.026, $\widehat{k_s}$ = 0.0005 and $\hat{b}$ = 0.05: (a) velocity; (b) concentration; (c) turbulent kinetic energy; (d) dissipation rate of turbulent kinetic energy; (e) eddy viscosity and (f) shear velocity

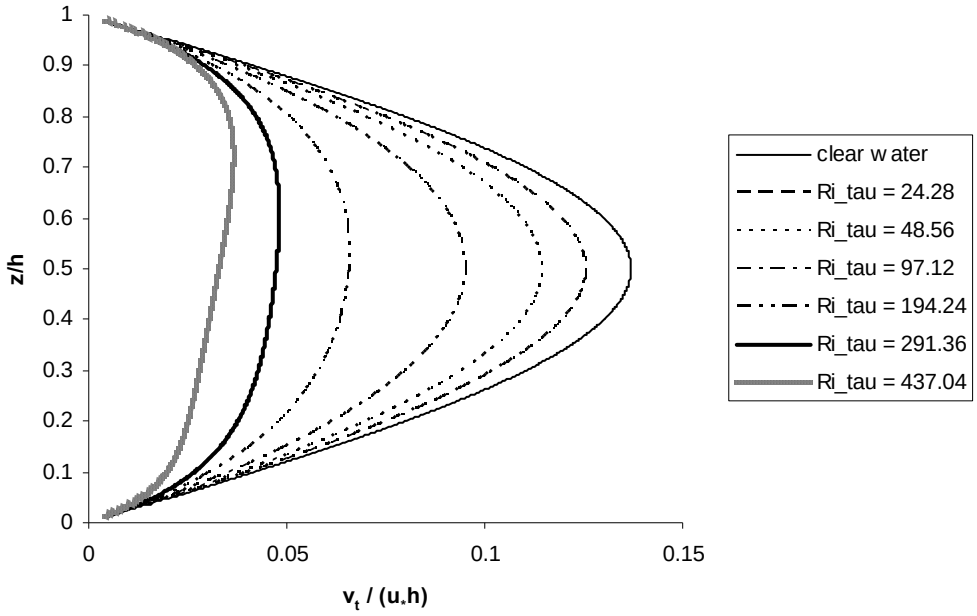

Figure 11. Eddy viscosity profiles for various values of Ri_τ, with $\widehat{\nu_s}$ =0.018

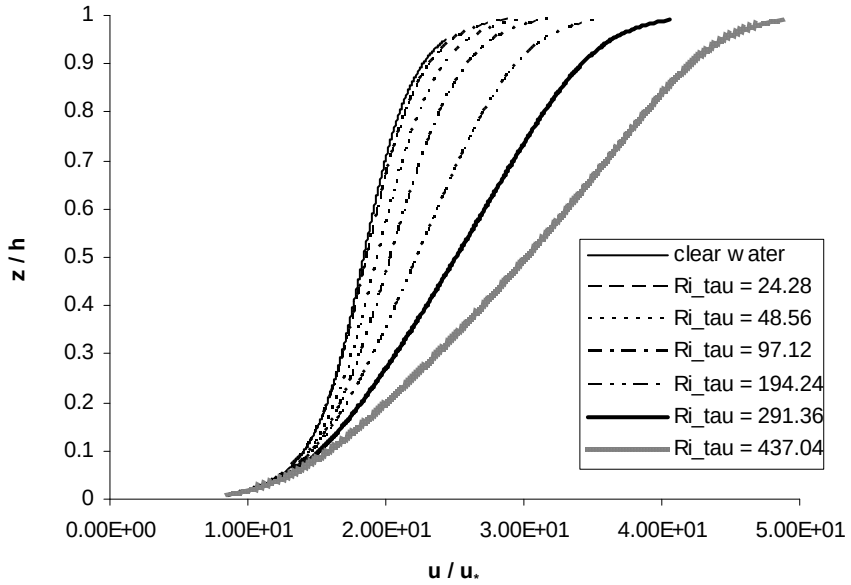

Figure 12. Velocity profiles for various values of Ri_τ, with $\widehat{\nu_s}$ =0.018

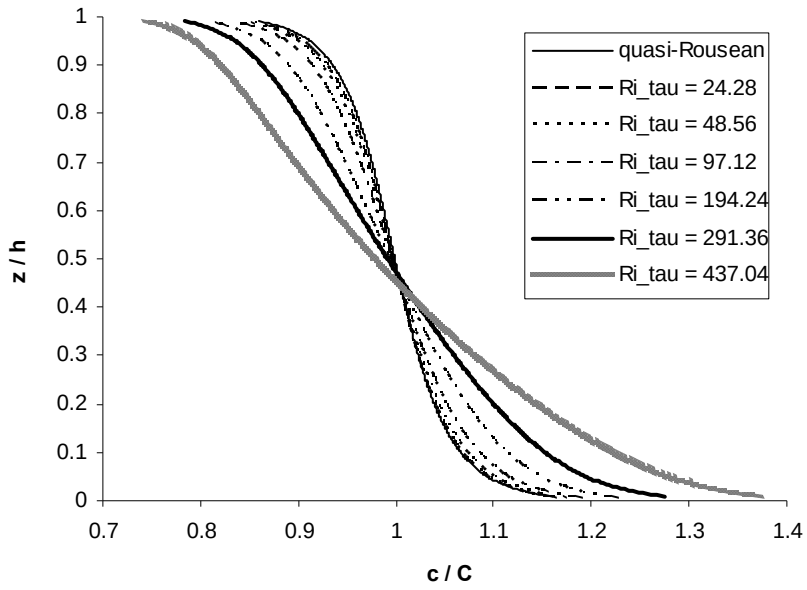

Figure 13. Concentration profiles for various values of Ri_τ, with $\widehat{v_s}$ =0.018

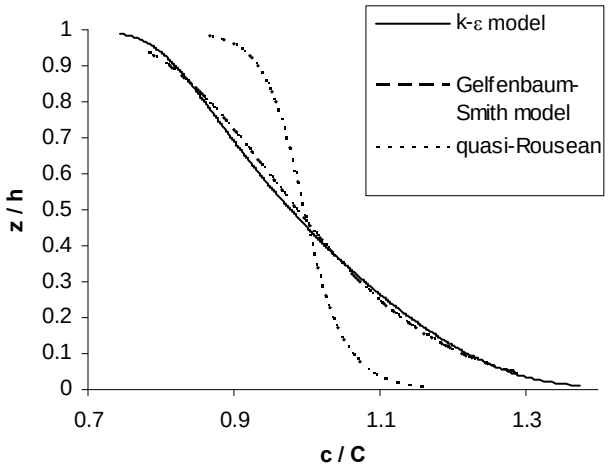

Figure 14. Concentration profiles obtained from the k-ε model, the Gelfenbaum-Smith model and the quasi-Rousean solution, for Ri_τ=437.04 and $\widehat{v_s}$ =0.018

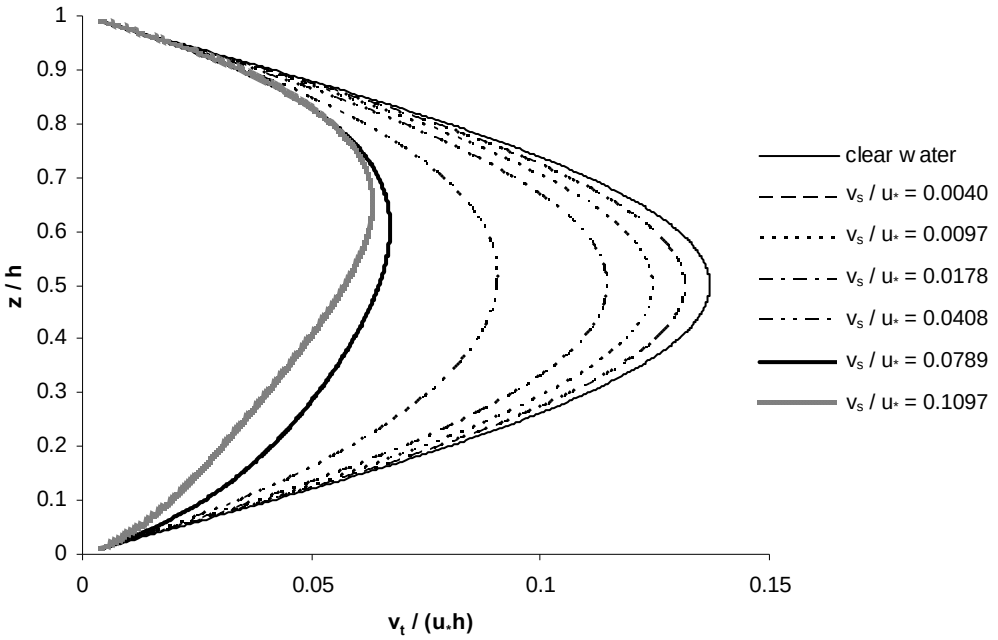

Figure 15. Eddy viscosity profiles for various values of $\widehat{\nu_s}$, with $Ri_\tau = 48.56$

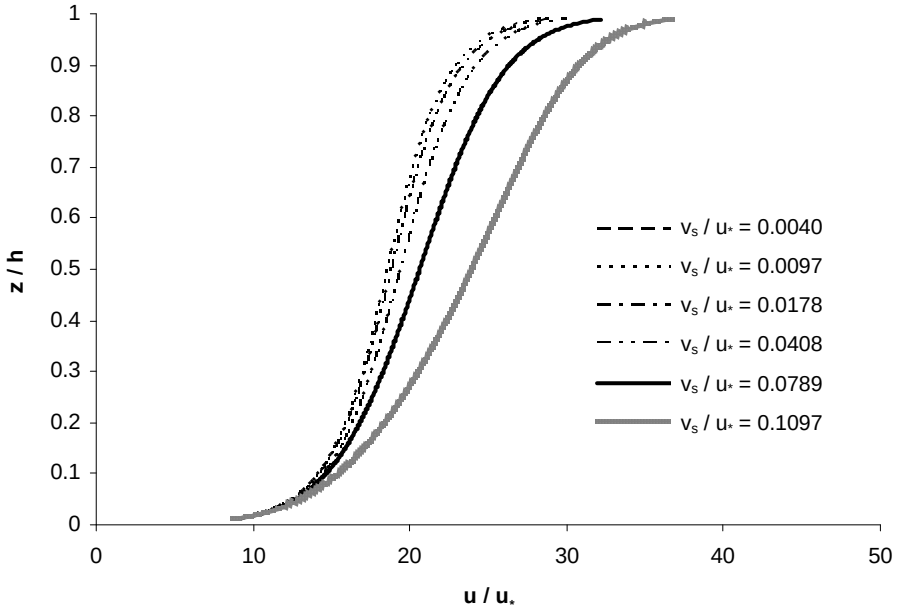

Figure 16. Velocity profiles for various values of $\widehat{\nu_s}$, with $Ri_\tau = 48.56$

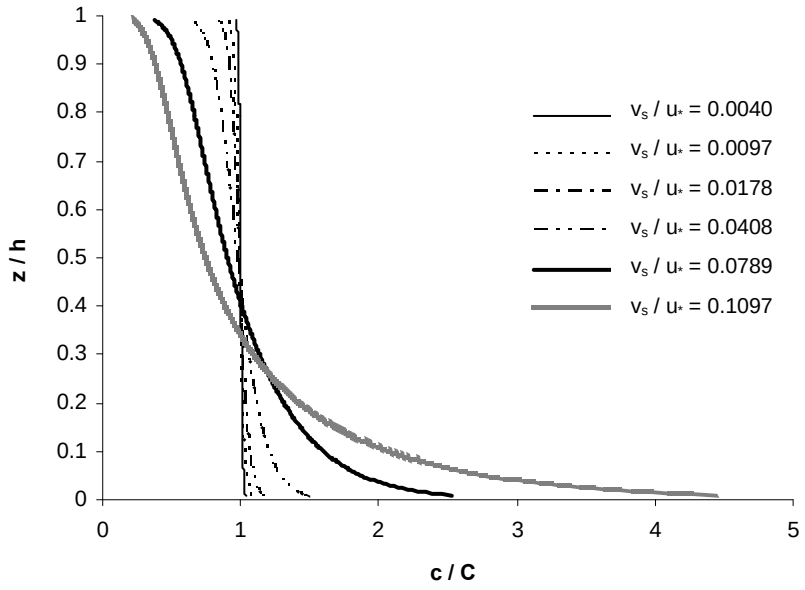

Figure 17. Concentration profiles for various values of $\widehat{\nu_s}$, with $Ri_\tau = 48.56$

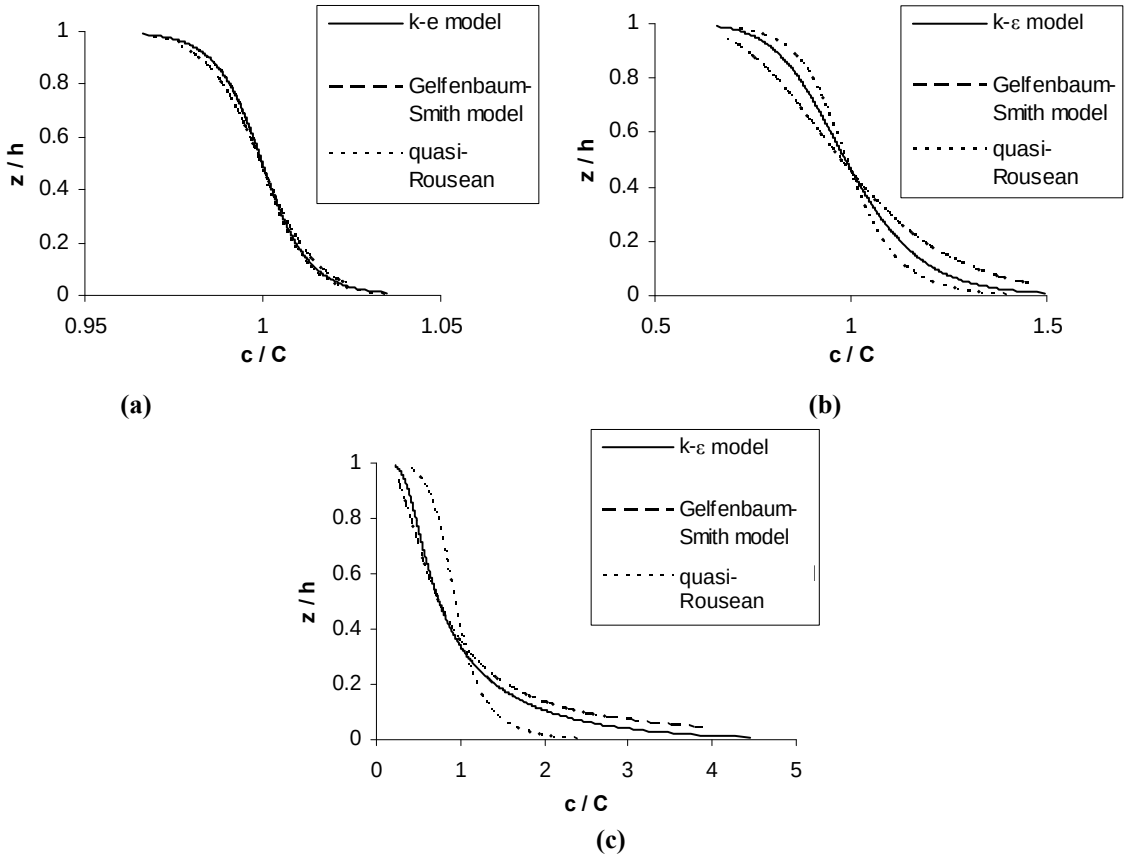

Figure 18. Comparison between concentration profiles predicted by the k - ε model, the Gelfenbaum-Smith model, and the quasi-Rousean solution: (a), $Ri_\tau = 48.56$, $\widehat{\nu_s} = 0.0040$; (b); $Ri_\tau = 48.56$, $\widehat{\nu_s} = 0.0408$; (c), $Ri_\tau = 48.56$, $\widehat{\nu_s} = 0.1097$

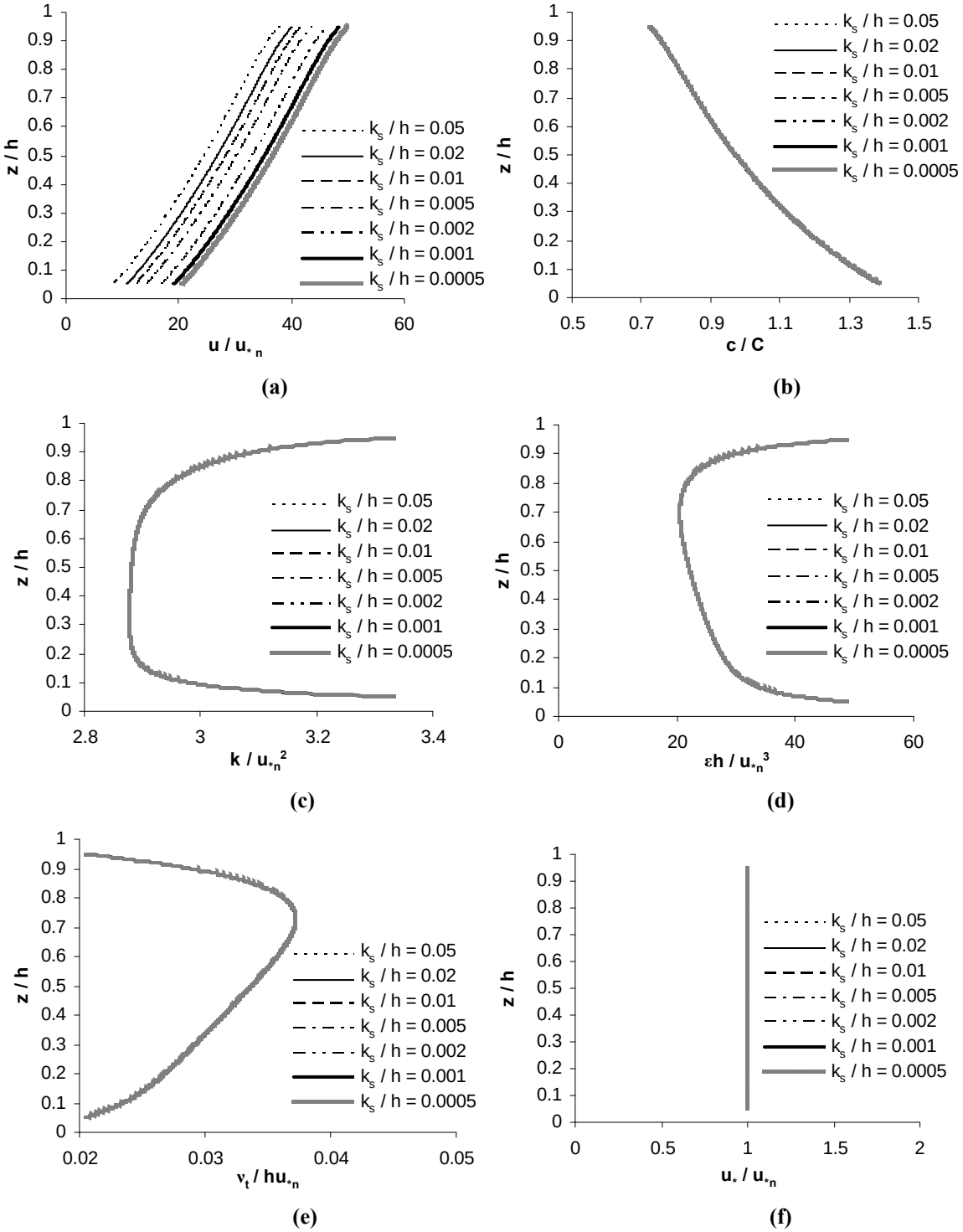

Figure 19. Comparison between simulation results of fully-stratified plane Couette flow with Ri_τ = 291.36 and $\widehat{\nu_s}$ = 0.026, with $\widehat{k_s}$ ranging from 0.0005 to 0.05, (a) velocity (b) concentration (c) turbulent kinetic energy (d) dissipation rate of turbulent kinetic energy (e) eddy viscosity (f) shear velocity

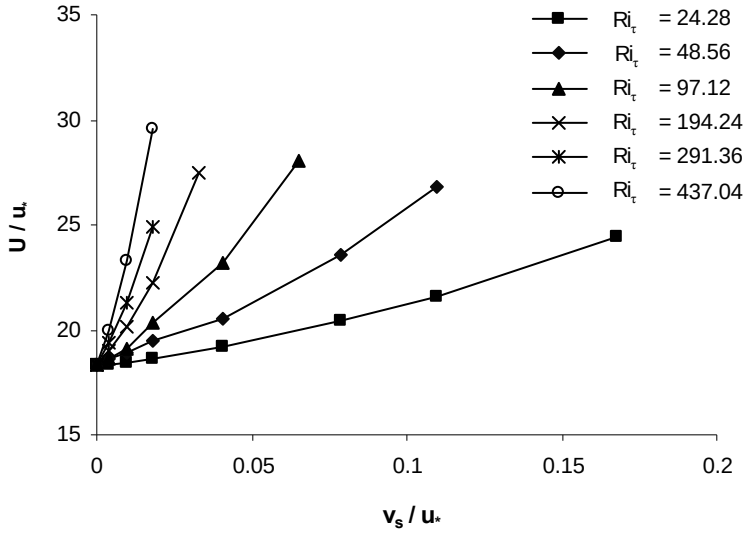

Figure 20. Relation of $\widehat{U}$ in plane Couette flow versus $\widehat{\nu_s}$ at specified values of Ri_τ

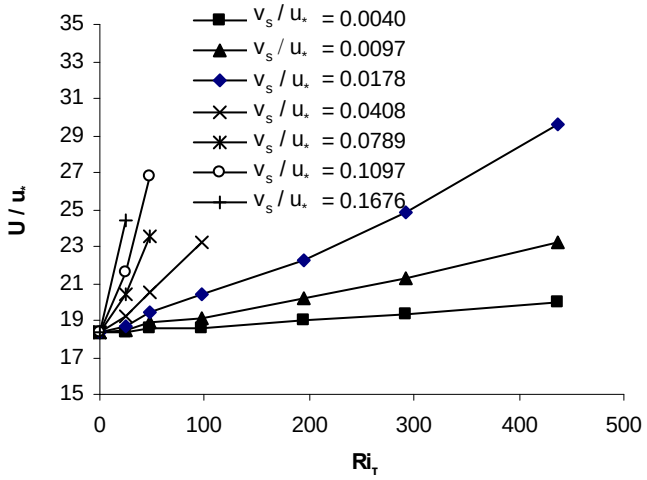

Figure 21. Relation of $\widehat{U}$ in plane Couette flow versus Ri_τ at specified values of $\widehat{\nu_s}$

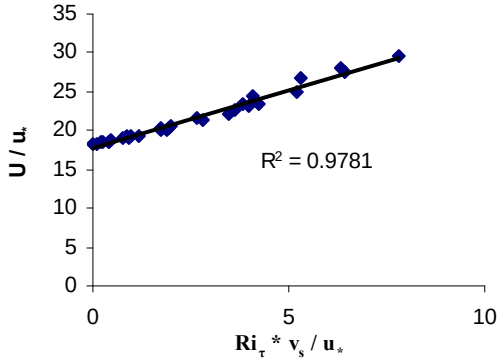

Figure 22. Relation of $\widehat{U}$ versus the product of $\widehat{\nu_s}$ and Ri_τ; the points are from the k-ε calculation, and the line was fitted by linear regression

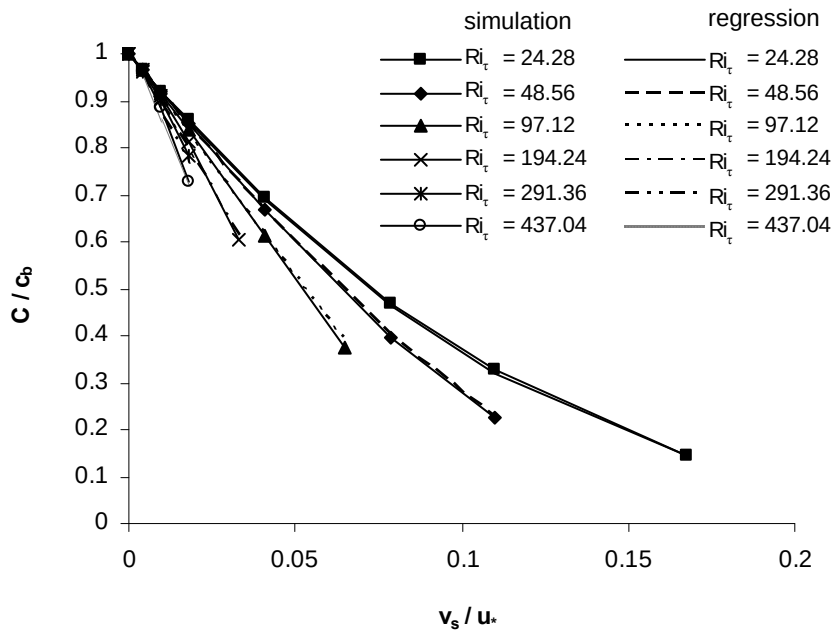

Figure 23. Relation of C/c_b in plane Couette flow versus $\widehat{v_s}$ at specified values of Ri_τ

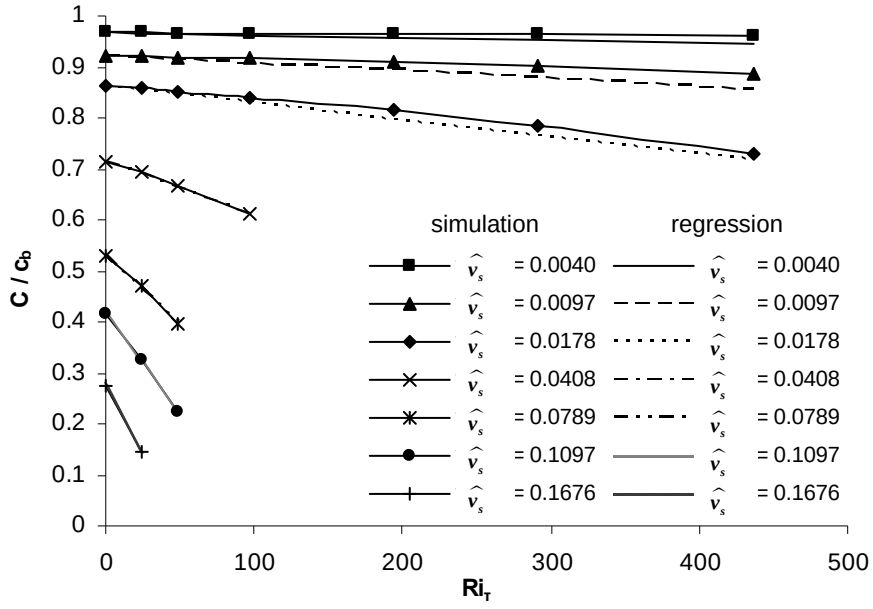

Figure 24. Relation of C/c_b in plane Couette flow versus Ri_τ at specified values of $\widehat{v_s}$

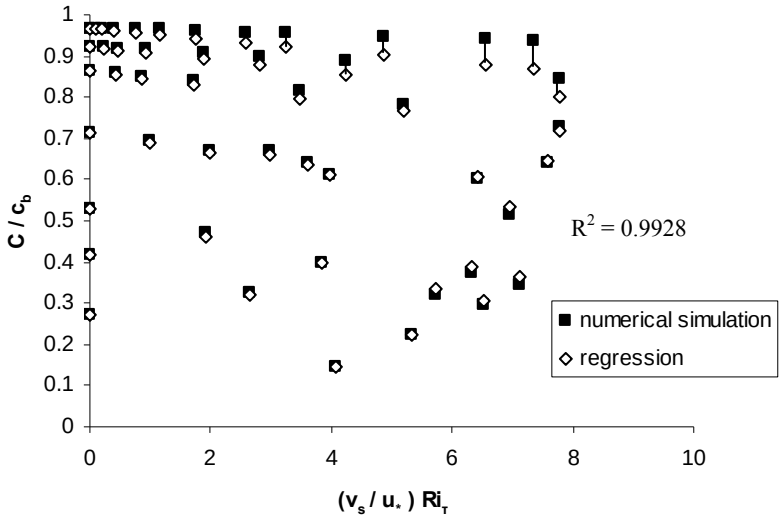

Figure 25. Plot of C / c_b computed with the regression relation (34), along with the results of the k-ε simulation, versus the product of $\widehat{v_s}$ and Ri_τ

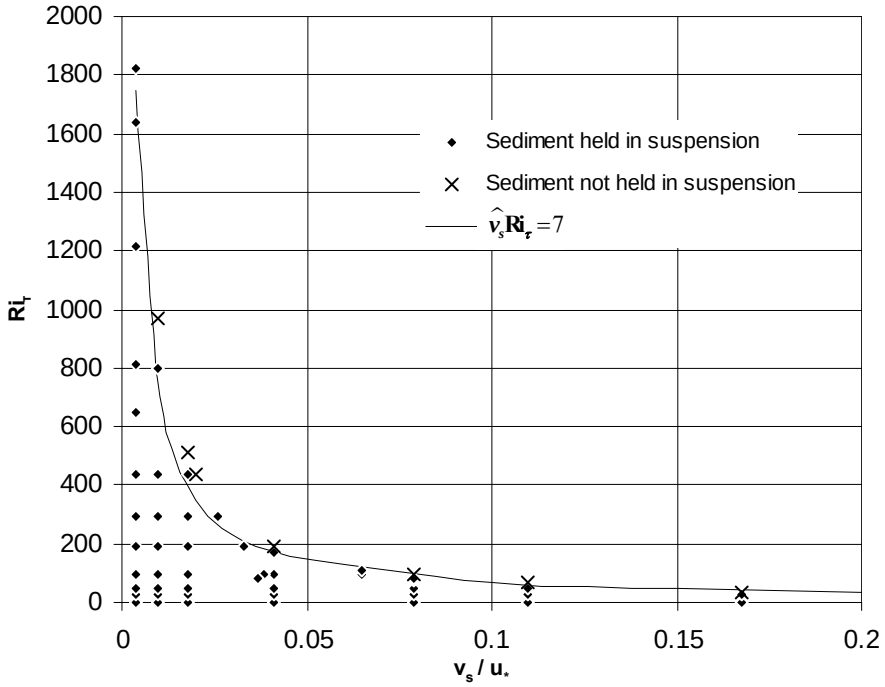

Figure 26. Criterion to hold sediment in suspension in the Ri_τ - $\widehat{v_s}$ plane

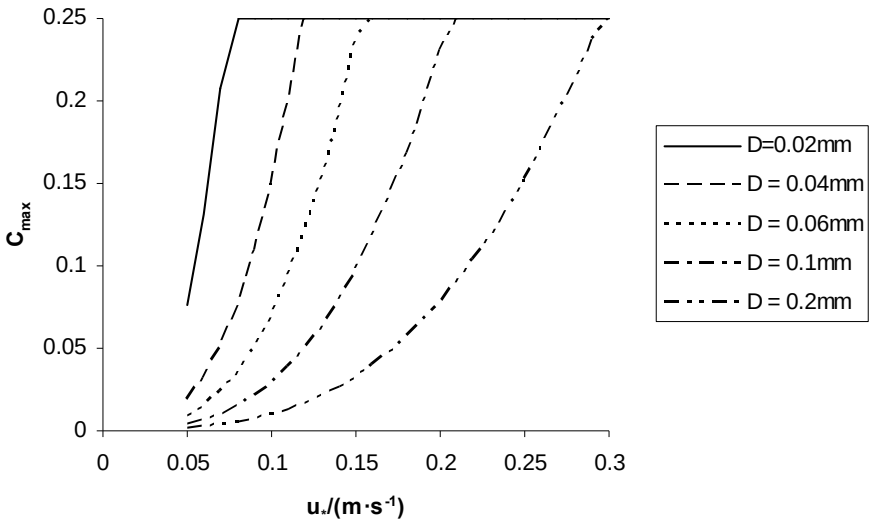

Figure 27. Maximum concentration in turbulent plane Couette flow for various grain sizes